

Numerical simulation and experimental evaluation for the development of a light electronic enclosure used in automotive industry

Susana Costa¹, Lourenço Bastos¹, Luciano Rietter¹, Rui Oliveira¹, Ricardo Freitas¹, Agnieszka Rocha¹, Bruno Vale¹, Carlos Ribeiro¹, David Serrão¹, Joana Silva¹, Nuno Gonçalves¹, Filipa Carneiro^{1*}, Susana Silva², Aníbal Portinha², Pedro Bernardo², Gustavo Dias³

¹ PIEP - Innovation in Polymer Engineering, Guimarães, Portugal

² Bosch Car Multimedia, Braga, Portugal

³ Polymer Engineering Department – University of Minho, Guimarães, Portugal

* corresponding author: f.carneiro@piep.pt

ABSTRACT:

The automotive sector is currently facing a paradigm shift, characterized by heightened demands in sustainability, emissions reduction, efficiency, and safety. Respond to these concerns is imperative, with the need to accelerate the implementation of production processes with minimized environmental impact and costs. This paper underscores the critical need for developing innovative lightweight solutions within the automotive industry. This entails a comprehensive reevaluation of components through redesign or the adoption of novel materials and advanced manufacturing techniques. The study aims to explore and propose strategies that align with the industry's evolving priorities, facilitating the swift adaptation to stringent standards while concurrently enhancing performance and sustainability across automotive applications.

This paper focuses on the development of a Lightweight Electronic Enclosure (LEE) achieved by substituting traditional metallic materials with functional polymeric and composite alternatives. The primary objective is to meet stringent product requirements while concurrently reducing weight relative to the established metallic baseline. Three critical functional prerequisites guide the development process: (1) ensuring the enclosure can withstand usage loads, (2) providing an effective thermal path for heat dissipation, and (3) isolating internal electronics from undesirable external influences while shielding adjacent devices from internal emitted radiations. The study outlines the methodology, materials selection, and performance evaluation criteria employed in the development of a lightweight yet robust electronic enclosure with enhanced thermal management and electromagnetic compatibility.

This study employs an iterative numerical methodology to support product development process. Using modeling and simulation resources, the approach aims to predict and evaluate the fulfillment of specifications. The simulation involves replicating relevant physics to emulate real-world conditions, enabling the assessment of mechanical strength, thermal dissipation, and electromagnetic protection in the LEE. This iterative numerical method enhances the accuracy and efficiency of predicting product performance, contributing to informed decision-making throughout the development lifecycle.

Following the production of functional prototypes, the product is subjected to a battery of experimental tests aimed at validating the simulation results. The assessments confirm the compliance of the overall product specifications. Significantly, a 33% reduction in weight is achieved, with corresponding expectations of cost and environmental impact reduction. This study validates the efficacy of an innovative simulation-based methodology, showcasing its capability to, systematically, reduce both the weight and cost of components. The findings underscore the potential for widespread application of this methodology in advancing cost-efficient and lightweight design practices across several industrial sectors.

Keywords: automotive industry, simulation, lightweight material.

1 INTRODUCTION

The development of lightweight products in the automotive industry has gained greater importance as environmental concerns grow, along with the need for cost reduction. Polymeric materials have been investigated for lightweight vehicles, giving evidence in weight optimization, with assurance of compliance with mechanical requirements [1, 2, 3]. The enclosures of automotive electronic devices present greater challenges, as in addition to mechanical performance, it is essential to ensure electromagnetic (EM) shielding [4, 5] and thermal management [6, 7], to guarantee proper operation and prevent interferences. Therefore, the development of a design concept that combines different materials, according to the specific requirements of each critical zone, is an important strategy, so that all mechanical, electromagnetic shielding and thermal requirements are met.

According to the book “Lightweight Polymer Composite Structures”, the invention of fast, responsive, smart, multifunctional and lightweight polymer composites has proved to be a boom in modern human civilization, and they are becoming more and more popular to meet the various needs of the rapidly evolving society. In order to mitigate several negative aspects of modern times, including unwanted radiation/noise pollution and energy crisis, the development and effective use of various polymeric, lightweight and smart materials are crucial in the areas of pollution reduction and unconventional energy sectors.

Electronic enclosures play a critical role in protecting sensitive electronic components in vehicles, ensuring their optimal performance and reliability. However, they must meet specific performance requirements to withstand the demanding conditions encountered in automotive applications.

An effective thermal management is required to prevent overheating and damage to internal components. Advanced cooling mechanisms, such as heat sinks, fans, and passive techniques, ensure the reliability and reliability of enclosed electronics.

These devices are also subjected to diverse mechanical stresses, including shocks, road vibrations, and impacts. The design phase requires considering these challenges through proper material selection, and structure reinforcement.

Automotive electronic enclosures must meet electromagnetic compatibility (EMC) requirements to prevent interference with and/or from other vehicle systems or external sources. The enclosure should incorporate electromagnetic shielding materials, and proper grounding techniques to minimize electromagnetic radiation emission and interference with nearby systems or radio frequencies.

Furthermore, the balance must be found between providing adequate protection and fitting in the available space in the vehicle. In addition, the development must comply with relevant industry standards and regulations, alongside the internal references provided by the manufacturers.

Meeting these performance requirements is crucial for reliable, long-lasting automotive electronic enclosures.

Accurate virtual simulations using CAE tools prior to prototype construction can help to early understand project risks and arrive at a reliable solution. The prediction accuracy of the simulation is driven by the inputs and modeling approach used in the analysis. This indicates that simplified modeling techniques aided with engineering assumptions are essential for virtual simulation.

2 DESIGN AND DEVELOPMENT APPROACH

The Lightweight Electronic enclosure was developed through an iterative approach. This development process emerged with the conversion of the already existent metallic device into some polymeric/composite model geometry, oriented to the productive process, selected materials, and all the defined requirements. After the working platform definition, some concepts were developed, analyzed and the best candidate was chosen. This first concept worked as the first iteration of the iterative process and consequently as a base for all subsequent dynamic mechanical, thermal, and EMC numerical simulations. Each iteration ended up with an improved CAD release based on the numerical simulations results. The following iteration started with the simulations of that new CAD release. This iterative process was defined as concluded by the end of the fourth iteration (fourth CAD release), as the simulations of this version fulfilled the requirements defined initially by the customer, that drove us to a confidence level to post experimental tests.

One of the main objectives is to reduce the weight of the enclosure, meanwhile maintaining the external dimensions to maintain the ability to be assembled into the system. This optimization will be done primarily by replacing the metallic materials of the equipment with functional polymeric and composite materials. To reduce weight without compromising the mechanical, thermal and electromagnetic characteristics of the equipment, materials are selected, and initial geometric concepts are generated, based on the original geometry of the electronic package. The concept is designed to aim for cost reduction without limiting the rest of the unit requirements. Next, some numerical simulations are made to ensure that the equipment's performance is always satisfactory. After the CAD release, an iterative cycle of simulations begins until all requirements are fulfilled.

For each simulation, some hypotheses are made for the initial conditions, operating conditions, constraints, material model and other convenient assumptions. Before analyzing any simulation, the mesh convergence is checked for each type of simulation. From an initial geometry, thermal simulations are performed with different types of flow rates, heat convection rate and a detailed analysis of the temperature evolution in each critical component. The heat management shall be capable of extracting the generated waste heat out of the component, to maintain the operability of the component under all operating and environmental conditions and prevent its thermal shut down.

Parallel to the thermal analysis, two types of structural simulations are also carried out: random vibration and drop test. The random vibration simulation is performed to assess the structural integrity and performance of the system when subject to a specific random vibration profile. The drop test simulation intends to test the impact of the equipment in a free fall, with the mechanical shock in which the components would be more susceptible to damage. Both numerical studies provided information to improve the design by identifying potential weaknesses and verifying that the structure can withstand the anticipated loads. The device must resist all mechanical loads without malfunction, permanent deformation, or damage when installed.

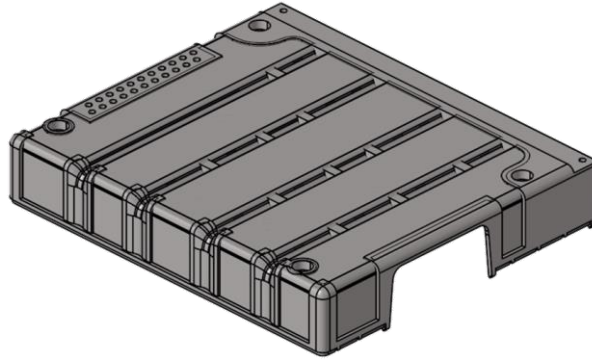
Concomitantly, an electromagnetic analysis (EMC) of the equipment, using the geometry that resulted from the previous thermal and structural simulations, is also carried out to predict the zones inside the enclosure where electric fields can be harmful to the proper functioning of electronic devices. With this, the steps to be taken are materials selection, design, numerical simulations and geometry optimization. The simulations presented in this work are relative only to the last iteration.

After this development stage, the final geometry is generated, a prototype is created, and an analysis of the process simulation is carried out. Finally, validation tests are performed, regarding mechanical, thermal and electrical performance.

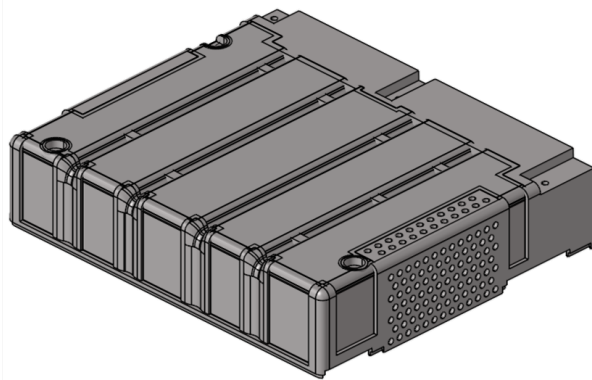
2.1 *Concept geometry*

The initial concept is based on the previous product, as compatibility with the current systems is desired. All the necessary adaptations in geometry were made to ensure a feasible change from metallic parts into polymeric\composite ones, despite the referred constraints.

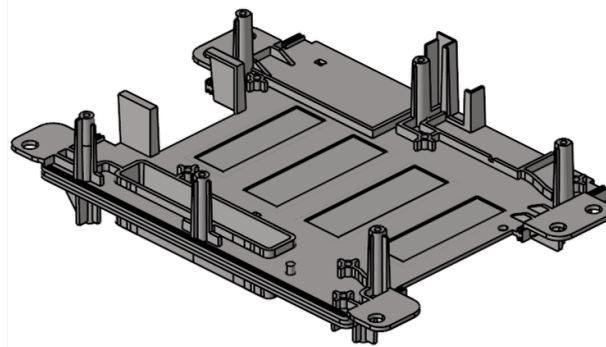
Figure 1 it is possible to observe the main parts used in the simulations.



a) Top part



b) Bottom part



c) Intermediate part

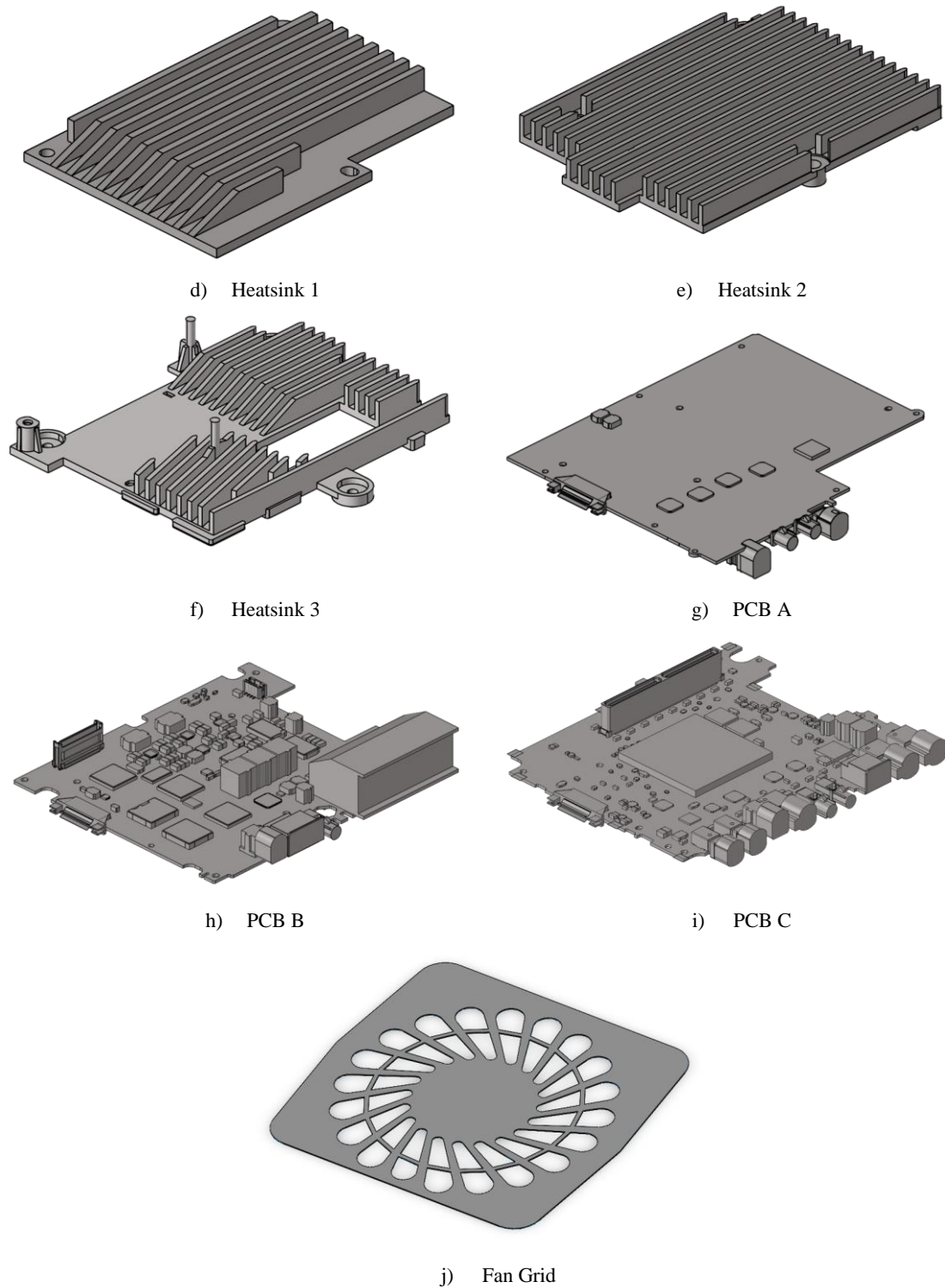


Figure 1 - View of the separated parts of the enclosure used in the simulations.

To decrease the computational load of the numerical simulations, the 3D models of the components have been geometrically simplified. Some examples of the geometric changes introduced are the elimination of some of the edge fillets in some locations of the housing and the removal of some areas with very tight ratio of curvature. Although these design elements are crucial for production, they can be challenging when building a consistent and structured finite

element mesh for numerical simulations. These simplifications have negligible effects and do not affect the reliability of the findings.

2.2 *Materials*

The developed solution of the housing parts is composed by two types of high-performance polymeric materials: an electrically conductive and a thermal conductive. The idea of using different materials is to improve the shielding effectiveness of the enclosure in combination with a better thermal management. As the physical parameters are different for each of these applications, it would be more difficult to obtain a cost-effective material that fulfills both areas simultaneously. Therefore, for guarantee the electromagnetic shielding properties the material selected is an electrically conductive thermoplastic injectable-grade material, combined with a composite material of continuous carbon fiber (CF) impregnated with a thermoplastic matrix. For the heatsinks and other dissipative parts, a thermally conductive injection-grade thermoplastic is selected. Furthermore, the top and bottom plates of the enclosure are also changed, being basically constituted by two plates: a polymeric plate and a carbon fiber reinforced thermoplastic composite (CFRTP) plate, also known as “prepreg”, which has a similar or better thermal and electrical behavior of typical plastics, offering a far superior mechanical behavior.

1 The properties used for modelling the material on the numerical model are presented in the following tables: in
 2 Table 1 and Table 2 are presented the parameters more related to the mechanical simulations, in

3 Table 3 the properties for the thermal simulations and in Table 4 the relevant parameters
 4 for the shielding simulations.

5 **Table 1 - Mechanical properties of thermoplastic materials considered in numerical simulations.**

Material	Material model	Density (kg/m ³)	Young modulus (MPa)	Poisson's ratio	Yield stress (MPa)
Electrically conductive polymer	Elasto-plastic Isotropic	1 360	12 800	0.4	84.7952
Thermal conductive polymer	Elasto-plastic Isotropic	1 850	7 500	0.4	19.4644

6

7 **Table 2 - Mechanical properties of the composite materials considered in the numerical simulations.**

Material	Material model	Density (kg/m ³)	E ₁ (MPa)	E ₂ (MPa)	E ₃ (MPa)	v ₁₂	v ₁₃	v ₂₃	G ₁₂ (MPa)	G ₁₃ (MPa)	G ₂₃ (MPa)
PCB (FR4)	Elastic Engineering Constants	1500	11800	11800	7500	0.27	0.11	0.11	4645.6	4645.6	3378.38
CFRTP	Elastic Lamina	1500	48000	48000	-	0.1	-	-	4000	2662	4000

8

9 **Table 3 – Material properties used in thermal simulations.**

Material	Density (kg/m ³)	Thermal conductivity (w/m°C)	Specific heat (J/kg°C)
Aluminum	2650	140	896
Electrically conductive polymer	1360	0.2	1500
Thermal conductive polymer (heatsinks)	1850	In-plane: 20 Through plane: 6	50 °C – 1180 85 °C – 1250 130 °C – 1330
Gap Filler	3100	3.5	800
PCB (50%FR4-50%Cu)	4500	200	385
CFRTP	1500	In-plane (x e y): 2.5 Through plane (z): 0.6	25 °C – 900 120 °C – 1291 200 °C – 1466

10 **Table 4 - Relevant properties for shielding simulations.**

Material	Relative Permittivity (ε _r)	Dielectric Loss Tangent (tan δ _e)	Electrical Conductivity (σ)	Relative Permeability (μ _r)	Magnetic Loss Tangent (tan δ _m)
FR4	4.3	0	---	---	---
Electrically conductive polymer	1	0	250*	---	---
CFRTP	1	0	7659	---	---
Stainless Steel	---	---	1100000	1	0

11

* It corresponds to the maximum value measured in [8].

The materials properties of the solid components used in the thermal simulations are based in the materials datasheets. Table 3 shows the materials properties used in the simulations. The thermal conductivity of the heatsinks is anisotropic and therefore, is defined to be higher in the direction of the fins and lower in the perpendicular direction of the fins. Thus, in the latter, the thermal conductivity is the same as the through plane one. For both, heatsinks and heatpads, a variable specific heat was considered, depending on the temperature. These different parts and their constitution are schematically shown in Figure 2.

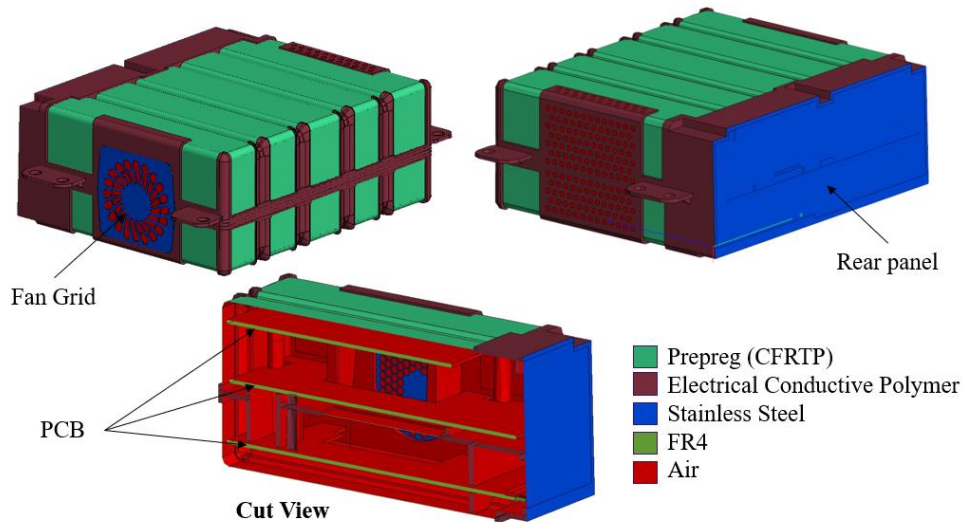


Figure 2 - Parts and materials used in the simulations.

3 THERMAL SIMULATIONS

One of the main objectives of this work is to decrease the weight of the enclosure through the replacement of metallic parts for polymeric ones. Since these materials normally present a much lower capacity to dissipate heat, several approaches are applied to compensate for this lack of thermal dissipation, with the objective of obtaining a thermal behavior similar to the metallic baseline. Using numerical simulations, it is possible to analyze the air flow and thermal behavior inside the enclosure and analyze different approaches to enhance its behavior without the need for continuous experimental testing and, consequently, reducing the costs associated with these.

These simulations are performed using the commercial software Fluent, from Ansys, which has proven capabilities for modeling flows, turbulence and heat transfer for several industrial applications.

This numerical model is implemented considering a convergence criterion of $1e-4$ and a turbulent flow, characterized by the standard k-Epsilon turbulence model, with enhanced wall treatment. Moreover, a steady state is considered for performing numerical simulations.

3.1 Approaches to enhance the thermal behavior

As mentioned before, the exterior enclosure and heatsinks, previously made of magnesium and aluminum, respectively, were changed to functional polymeric base materials, which has a great impact in the enclosure thermal behavior. Although locally these changes would not increase temperatures considerably, the sum of all changes would considerably affect the overall thermal performance of the enclosure. Thus, some approaches were applied to counterbalance these changes.

An approach also applied in the top and bottom plates of the enclosure was to add heatpads in these faces, whose material is the thermal conductive polymer. These heatpads are also connected to some heat sources, to help dissipate heat from the PCBs and from the interior of the enclosure, since its material has better thermal properties than the electrically conductive material and the CFRTP.

Also, in the top and bottom zones of the enclosure, several dedicated holes were added to the exterior enclosure to allow better air flow inside and increased air flow on the inlet. This allowed to greatly enhance thermal behavior inside the enclosure, particularly in the zones near the top face that had a considerable increase in temperature with all the material changes.

Furthermore, the heatsinks' geometry was redesigned so its thermal efficiency would be enhanced/optimized. The most notable change was made to the fins of the heatsinks, where its orientation was changed to enhance the air flow in specific zones with higher temperatures.

Finally, the airflow speed had to be increased by 25%, to enhance the thermal behavior. For the numerical simulation, this increase was done by changing the characteristic curve of the fan. In reality, this means that the fan had to be changed to a more powerful one. The results were also compared to the temperature limits defined in the datasheets of each electronic component, to check if any temperature was above the limit, which would invalidate the concept.

3.2 Geometrical model discretization

The geometrical model discretization in small control volumes, or mesh creation, is of utmost importance in a numerical analysis. When the mesh is adequate, the numerical solution is robust and efficient, and an accurate numerical solution is achieved.

The properties of the meshes created for the numerical thermal simulations are presented in Table 5. The total number of elements in the model were 36328317. Figure 3 presents a cut view from the mesh created for the simulations.

Table 5 – Mesh properties for thermal simulations.

	Material	Type	Element Size
Solids	PCBs	Hexahedrons (8 Nodes)	In-plane: 1.5 mm Through plane: 0.6 mm
	Heatsinks	Tetrahedrons (4 Nodes)	Global: 0.7 mm with proximity of 0.5 mm
	Gap fillers and heat sources	Hexahedrons (8 Nodes)	Global: 0.8 mm Thickness: 0.2 mm
	Composite plates	Hexahedrons (8 Nodes)	Global: 0.5 mm Thickness: 0.1 mm
	Enclosure and heatpads	Tetrahedrons (4 Nodes)	Global: 1.5 mm
Fluids	Air	Tetrahedrons (4 nodes) and Wedge elements for the boundary layer (6 Nodes)	Boundary layer: 3 layers, 0.2 mm for the first layer and growth rate of 1.2 Global: Tetrahedrons, 1.5 mm with proximity of 0.5 mm

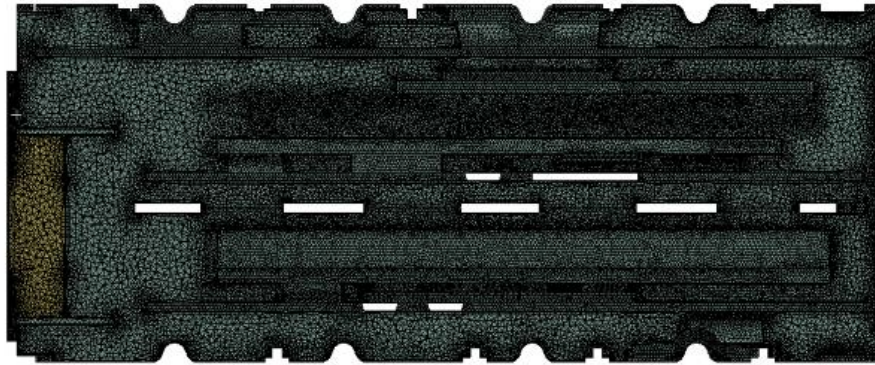


Figure 3 - Cut view of the mesh created for solid components and air.

3.3 Fluid properties

Besides the materials identified in Chapter 2.2, fluid materials were also considered for thermal simulations. For the air inside the concept, variable density and thermal conductivity, depending on the temperature, are considered. The air properties used in the simulations can be seen in Table 6.

Table 6 – Air properties used in the simulations.

Temperature (°C)	Density (kg/m³)	Thermal conductivity (W/m°C)	Specific heat (J/kg°C)	Viscosity (kg/m.s)
20	1.204	0.0262	1006.43	1.79E-05
50	1.093	0.0242		
80	1	0.03		
125	0.8868	0.0336		

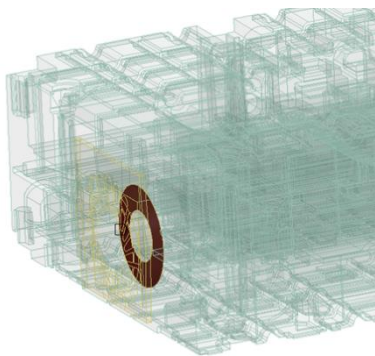
3.4 Simulation conditions

The boundary conditions and velocities are applied so simulations as similar as possible to reality would be obtained.

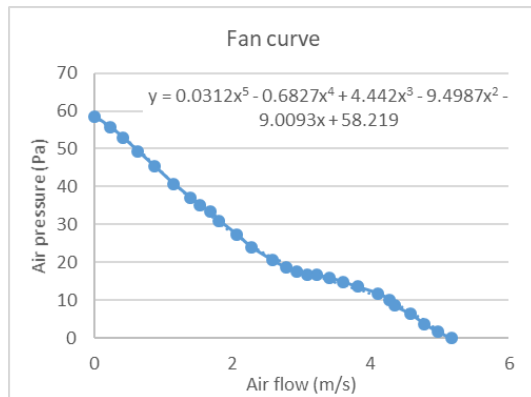
Starting with the boundary conditions, convection is applied in all the outer walls to simulate the air surrounding the lightweight enclosure, being defined a Heat Transfer Coefficient of $10 \text{ W/m}^2\text{°C}$ for a free stream temperature of 65 °C .

Furthermore, the power of each heat source is applied on the model through power density, obtained by dividing the power of the heat sources by the corresponding volumes.

To simulate the fan action, a fan surface boundary condition is defined, at the center of the fan (Figure 4a), by a polynomial function that describes the characteristic curve of the fan or P-Q curve (Figure 4b).



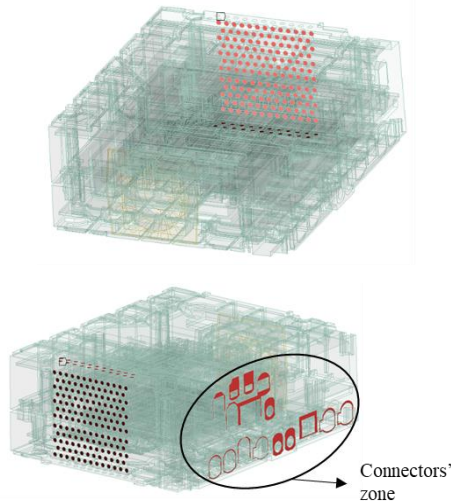
a)



b)

Figure 4 - a) Fan surface; b) Fan characteristic curve and polynomial function.

For the inlets shown in Figure 5a, a pressure inlet boundary is defined, with a turbulent intensity of 20% and turbulent viscosity ratio of 10. As for the outlet, shown in Figure 5b, pressure outlet boundary is defined, with a backflow turbulent intensity of 5% and a backflow turbulent viscosity ratio of 10.



Connectors' zone

a) Inlets

b) Outlets

Figure 5 – Inlets and outlets surfaces.

3.5 Results

The temperatures of the initially developed concept were analyzed, and it was observed that some of the temperatures in the electronic components were surpassing the temperature limits established in the datasheets. Thus, the geometry of the concept was modified in some areas to allow an enhancement regarding the thermal dissipation capacity.

The results presented here refer to the final geometry for the enclosure. Figure 6a shows an overview of the temperature distribution obtained in the enclosure and Figure 6b shows the temperature distribution for a cut plane, passing through the middle of the enclosure.

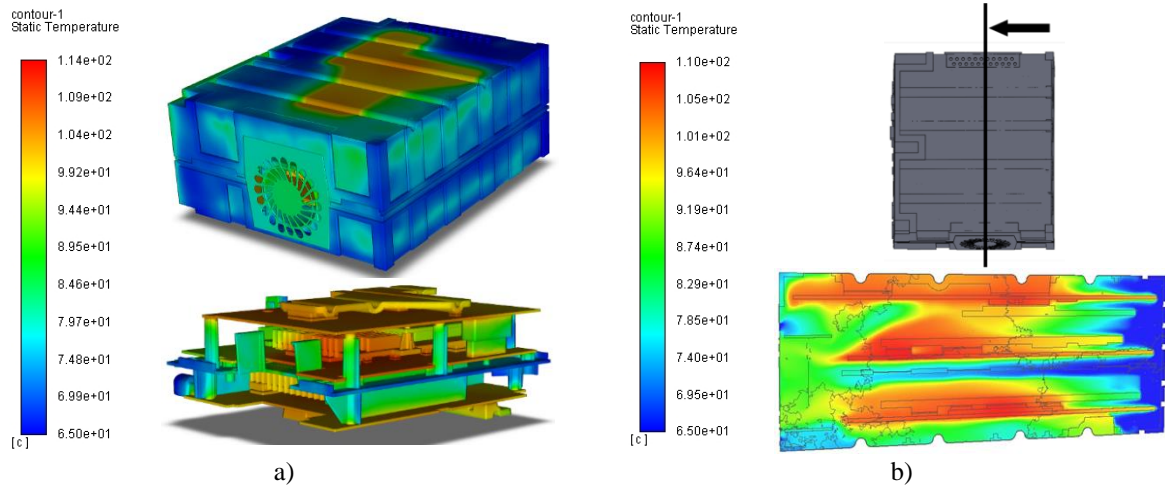


Figure 6 - Overview of temperature distribution in the enclosure (a) and (b) the temperature distribution in the cut plane.

As can be seen, firstly from the temperatures in the outer walls, these do not seem to have considerably high temperatures, being the highest temperature observed for the heatpad. Then, observing the temperatures inside the enclosure, the highest temperatures are observed in the zones around the heat sources, more specifically in the zones that are furthest away from the air inlets, which was expected. Moreover, this behavior seems to be similar for all 3 PCBs with the middle PCB having slightly higher temperatures.

To further analyze the temperature distribution inside the enclosure, Table 7 presents the average, maximum and minimum temperatures observed for the main volumes that constitute the enclosure.

Table 7 - Temperatures observed in the volumes (final concept).

Part	Final concept temperature (°C)		
	Average	Max	Min
Air	85.04	113.66	64.56
Shell top / Top cover	77.37	104.58	65.01

Shell bottom / Bottom cover	75.95	104.36	65.04
Chassis	83.29	105.37	65.06
Composite bottom / Bottom cover prepreg	77.11	103.39	65.00
Composite top / Top cover prepreg	77.78	95.95	65.75
Composite chassis / Chassis prepreg	82.91	105.82	65.63
Heatpad bottom	94.90	106.05	85.57
Heatpad top	103.03	107.72	97.93
Bottom heatsink	97.47	109.03	77.94
Intermediate heatsink	100.61	112.39	84.27
Top heatsink	93.52	107.24	80.68
PCB C	103.42	109.52	98.63
PCB B	102.91	113.20	93.96
PCB A	104.90	110.07	100.33
Plate connectors	91.71	98.61	75.07
Grill	82.80	85.77	80.82

Furthermore, in Table 8 are presented the temperatures observed for all the electronic components attached to PCB C and the limit temperature defined for each one of these components. Similar results are also obtained for the other PCBs.

Table 8 - Temperatures in the ICs in PCB C.

PCB SIDE	Component ID	Power	Operational Limit (°C)	Final Concept (°C)
TOP SIDE	3	1.58	125.00	104.11
	4	0.75	105.00	107.08
	5	0.75	105.00	106.64
	6	0.975	125.00	101.75
	16	1.175	150.00	102.31
	17	0.687	125.00	104.88
	18	0.55	125.00	104.88
	30	0.39	125.00	103.85
	33	0.2	150.00	100.43
	55	0.94	105.00	107.53
	52	1.5	125.00	107.77
	53	13.75	122.00	109.86
	54	1.5	125.00	107.61
	51	0.94	105.00	106.02
	57	0.125	150.00	102.06
	58	0.25	150.00	100.83
63	0.17	125.00	102.73	
BOTTOM SIDE	7	0.55	125.00	101.50
	8	3.4	150.00	106.99
	34	0.2	150.00	100.41
	49	1.73	125.00	104.64
	50	1.73	125.00	104.42
	64	0.036	122.00	105.77
	65	0.144	122.00	106.61

Analyzing the table, there are only a few components whose temperature are slightly above the limit, which is not considered to be problematic, and no components with temperatures considerably above the limit. In this case study, all components are considered to be working at the same time, which almost surely will not happen in reality, subjecting the enclosure to a far more demanding thermal load than the load that will ever be applied during normal usage.

4 STRUCTURAL SIMULATIONS

We propose conducting structural simulation studies to validate and assess the mechanical performance of the lightweight electronic enclosure housing. The goal is to ensure that the housing can withstand the mechanical stresses and forces it will encounter throughout its operational lifespan. By subjecting the housing to simulated mechanical conditions, we can evaluate its structural integrity, pinpoint potential weaknesses, and make design improvements as necessary.

In this study, we perform two distinct mechanical tests to evaluate the mechanical behavior of the device. Specifically, we conduct dynamic behavior analysis, which includes two separate simulations: random response analysis and structural analysis following a free-fall impact.

The random response simulation aims to replicate the vibrations experienced by the device when it is in motion within a vehicle. By analyzing the acceleration and displacement power spectral density (PSD) and root mean square (RMS) responses at critical points of the device, it is possible to evaluate its ability to withstand and dampen vibrations effectively.

The Free-Fall Impact simulation allows to assess the device's ability to withstand impact forces and evaluate its structural integrity after impact. The falling housing is evaluated in four distinct configurations, each falling on a different side, to provide comprehensive insights.

Both evaluations contribute to the device's mechanical design being optimized and assuring its strong performance in real-world automotive applications.

The commercial software ABAQUS® is used to build the finite element models.

4.1 Geometrical model discretization

Creating the finite element mesh is a complex non-linear process that involves striking a balance between obtaining accurate results and minimizing computational resources. The structural mesh generated for this study has a general element size of 0.6 mm. Table 9 provides information on the type and total number of elements for all model components, and Figure 7

displays their respective finite element meshes. The total number of elements in the model amounts to 9,769,195.

Table 9 - Type and total number of elements in global numerical model components.

Material	Type	Element Size
PCBs	Hexahedrons (8 Nodes) and wedge (6 Nodes)	0.6 mm
Heatsinks	Tetrahedrons (4 Nodes)	0.6 mm
Composite plates	Quadrilateral (8 Nodes) and triangular (6 nodes)	0.6 mm
Enclosure and heatpads	Tetrahedrons (4 Nodes)	0.6 mm

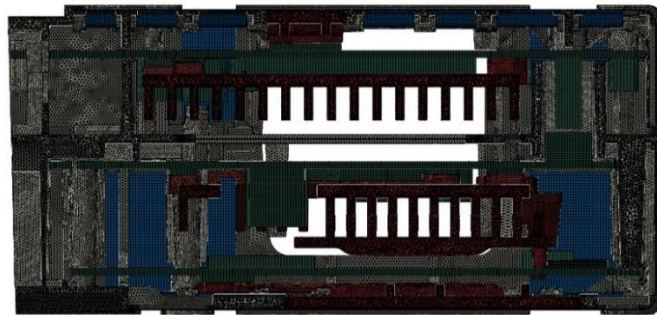


Figure 7 - Finite element mesh of the main components.

4.2 Random vibration

Random response analysis evaluates the dynamic response of the structure when subjected to random vibrations. During vehicle operation, the perceived loads cannot be precisely defined due to their complex random nature. The severity of a random vibration phenomenon is usually described in terms of a power spectral density (PSD) function which provides information about the distribution of power across different frequencies in the vibration signal. This function is a statistical representation of the experimentally determined load time history.

This analysis determines the root mean square (RMS) accelerations and displacements that result from constant random vibration over time.

Random vibration analysis uses a mode superposition method that requires inputs from linear natural frequency analysis or modal analysis. Therefore, an initial modal analysis was performed to acquire the dynamic characteristics of the enclosure. The electronic enclosure natural frequencies and mode shapes were primarily obtained to subsequently perform spectrum response analysis.

4.2.1 Simulation conditions

The enclosure boundary conditions are implemented according to the test condition. The connections between components are made mostly using screws. The approach used in the PSD simulations is to consider rigid connections between all components using, for that purpose,

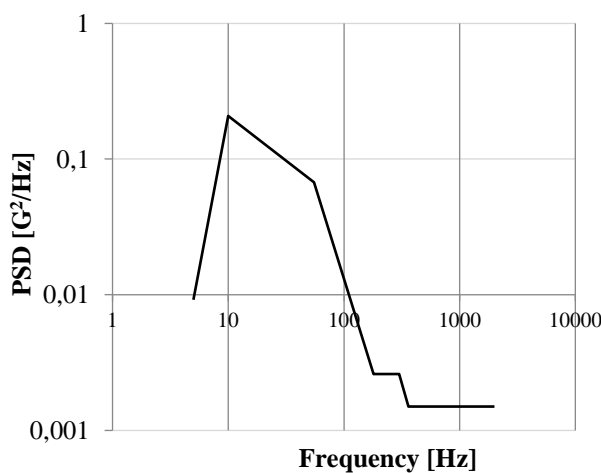
TIE connections formulation in the finite element software. Throughout the simulation, all nodes that are initially in contact will remain connected. The lateral mounting points are constrained in all degrees of freedom (X, Y, and Z), as can be seen in Figure 8.



Figure 8 - Boundary conditions on the model.

As previously stated, modal analysis is performed first to do a spectrum response analysis using the mode superposition approach. According to the finite elements' analysis methodology, the modal analysis solves the problem of free vibrations having as a base the principle of energy conservation and the second Newton's Law. The system is excited for one instantaneous and linear perturbation and vibrates freely. The component vibrates at its natural frequency if the system is neither dampened nor subject to external influences. The type of analysis defined in the application of finite elements for the execution of modal analysis is the "linear perturbation step". The model is evaluated in the frequency domain for resonance frequencies and mode shapes. The natural frequencies and mode shapes are extracted for a frequency range from 5 Hz to 3000 Hz. The maximum frequency is well above the maximum excitation frequency of the PSD to correctly rebuild the system response from the modal response.

A power spectrum density plot must be given to run a random response numerical simulation. The PSD profile used to configure the random response simulation can be seen in Figure 9. The numerical analysis software takes PSD profiles in terms of acceleration of gravity (G^2/Hz) (base motion).



Frequency [Hz]	PSD [$m/s^2/Hz$]	PSD [G^2/Hz]
5	0.884	0.0092
10	20	0.208
55	6.5	0.0676
180	0.25	0.0026
300	0.25	0.0026
360	0.14	0.0015
1000	0.14	0.0015
2000	0.14	0.0015
RMS acceleration	30.8 m/s^2	3.14 G_{RMS}

Figure 9 - PSD profile used in random response simulations.

It is also assumed a damping coefficient over the range of calculated Eigenmodes.

After establishing the numeric model, the response outcomes under random vibration excitation are calculated. The PCBs' dynamic response, root mean square acceleration, displacement, and PSD response are tested. The output responses are statistical in character, as are the input excitations.

4.2.2 Results

A random response numerical analysis provides two types of results: PSD response and RMS response. The PSD response characterizes the amount of power per unit of frequency of the system in terms of acceleration or displacement, while the RMS (root mean square values) shows the probability of occurrence of the corresponding acceleration or displacement values. It is usual practice to consider the three sigma values when designing. Figure 10 exhibits a comparison of input PSD and output PSD at different locations.

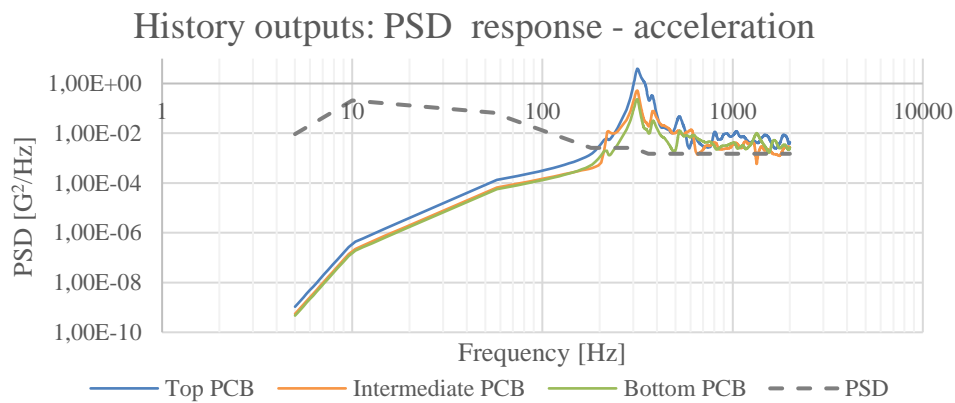


Figure 10 - PSD acceleration response versus input acceleration PSD.

The acceleration response energy of the system is less than the energy delivered to the system at all measuring locations between 10 Hz and 180 Hz. This indicates that vibrations in the frequency range have little effect on the system. An enhancement of the system oscillatory response is found at higher frequencies (>180 Hz), which coincides with several of the system resonance frequencies. Although there is a significant possibility that the system may approach resonance, these are frequencies with a low probability of occurrence, hence the low energy involved; thus, the results can be considered non-critical. Figure 11 shows the acceleration and displacement results.

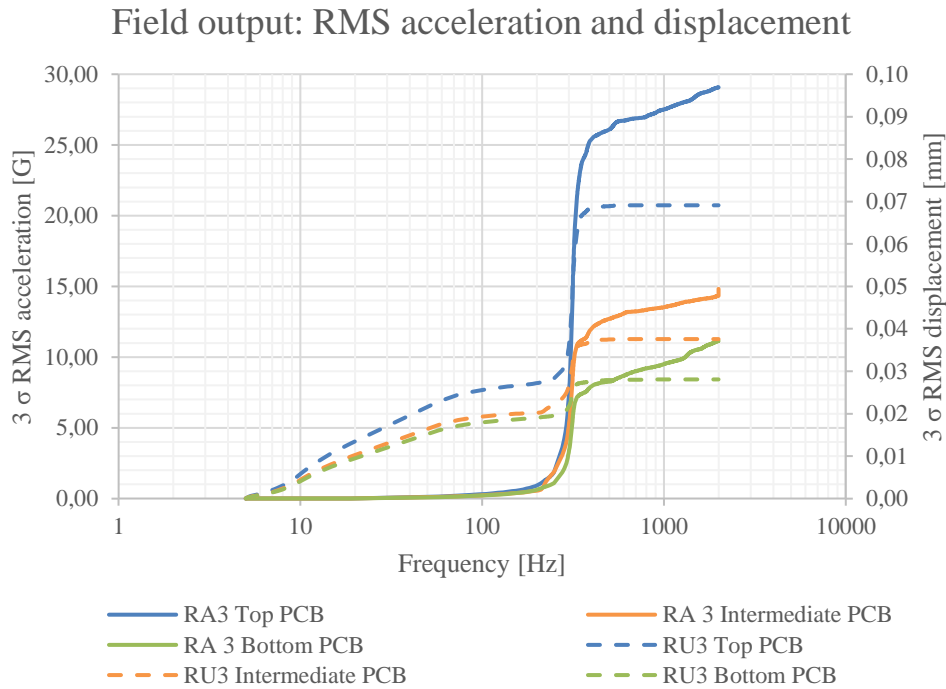


Figure 11 - RMS acceleration (RA) and displacement (RU) results.

The 3-sigma results of acceleration and displacement show that there is a 99.73% probability that the corresponding time history for these quantities will not exceed the maximum (at each frequency unit) value determined in the simulations. The top PCB is the component with the highest displacement and acceleration values of all the measuring points considered, maximum displacement values of 0.069 mm and maximum acceleration of 29 G. The achieved results for intermediate PCB show a maximum displacement value of 0.037 mm and maximum acceleration of 14.8 G. In bottom PCB the maximum displacement and acceleration is 0.028 mm and 11 G, respectively. These displacements values are lower than the critical ones, which can cause PCB strains leading to damage or malfunction of the electronic components.

4.3 Free-fall

The primary goal of this simulation is to evaluate the structural integrity of the developed polymeric housing when subjected to a drop test. This test replicates the free fall of a device to the floor, as it may occur throughout the entire process chain until the planned mounting on the vehicle.

After modeling the free fall of a polymeric housing from 1.2 meters in height, a structural study is carried out. The falling housing is evaluated in four possible configurations, each falling on a different side, to provide comprehensive insights.

4.3.1 Simulation conditions

As the random response numerical model [CRI], TIE connections are used to model the connections between parts. This approach yields acceptable results throughout the model; however, some locations are expected to show high stress values, especially on elements around fastening holes. This is caused by the numerical rigidity induced by the TIE connections, which in the end has a negligible effect on the final results.

There are contacts defined between the components of the housing and with the rigid surface representing the impact floor. For the contact properties normal behavior was defined as “hard contact”. Impact floor is represented as rigid surface with all degrees of freedom constrained. As a predefined field, a velocity of 4852 mm/s, indicating a drop from 1.2 m height, is applied to the housing. The acceleration of gravity (9810 mm/s^2) is also considered in this simulation. Four falling housing configurations are evaluated, two orientations (y and z) and both sides. Figure 12 illustrates them all.

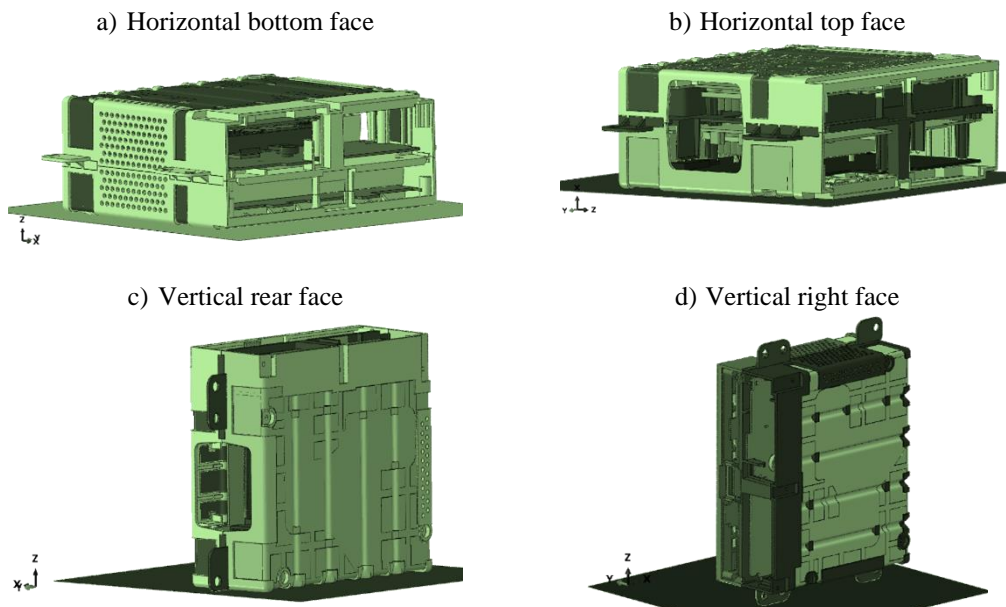


Figure 12 - Four configurations of free-fall simulations.

4.3.2 Results

The deformation and stress distribution within the enclosure parts after impact was analyzed. The simulation results will be compared with the allowable yield stress of materials, which may be found in Table 1, and the high-stress concentration and potential failure points were identified.

Figure 13 and Figure 14 show the worst distribution of von Mises stress in major parts of the housing due to free fall.

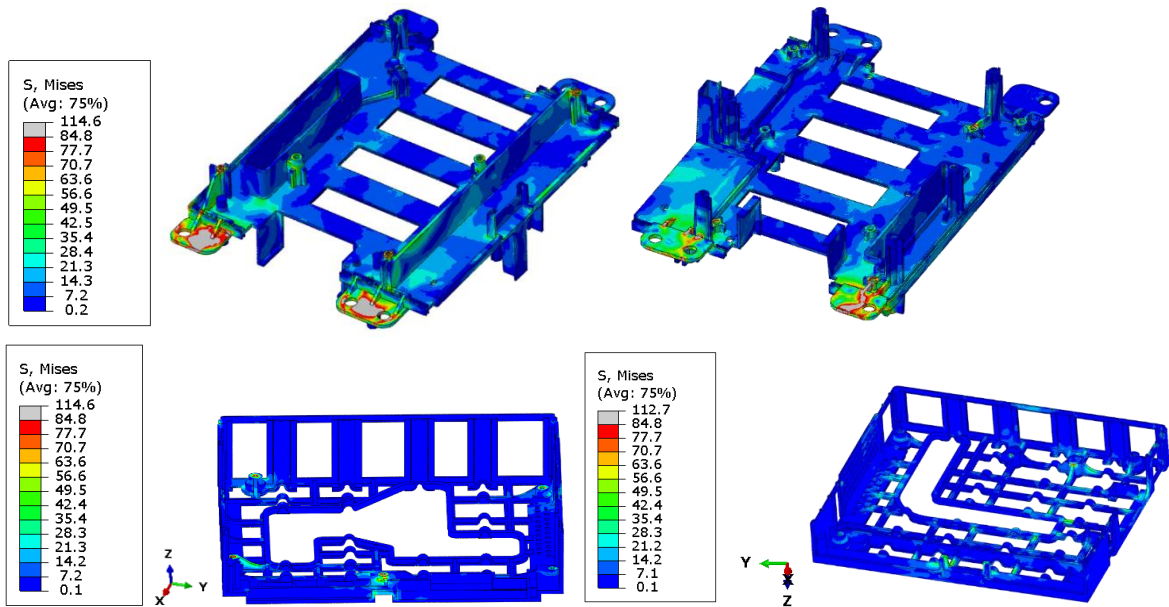


Figure 13 - Von Mises stress in structural housing components: top, bottom, and intermediate.

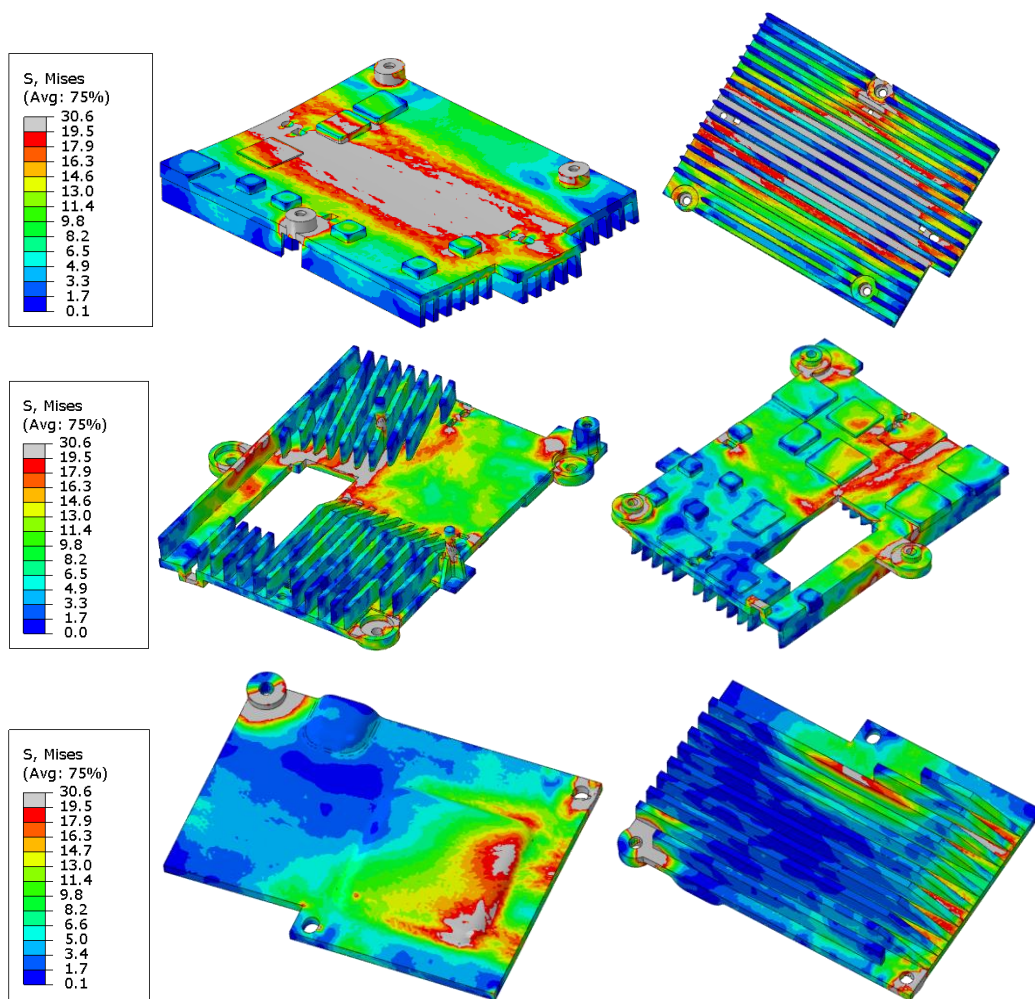


Figure 14 - Von Mises stress in Bottom (top), Intermediate (middle) and Top (bottom) Heatsinks.

According to the results of the analysis performed on the four distinct free-fall scenarios, all structural components of the enclosure exhibit good integrity. At a localized level, it is noteworthy that certain areas experience stress levels surpassing the yield value of 84.8 MPa. It occurs due to the inherent higher stiffness introduced by the simplifications applied during the modelling process. These elevated stress levels arise primarily at the points where several parts come into contact with each other, and also in fixing pins regions.

The heatsinks demonstrate weaknesses in several areas such as fastenings, pins, geometrically weakened areas (big cuts), and contacting surfaces, presenting in large areas stress value higher than the material yield stress, 19.5 MPa. As a result, corrective actions are taken within the constraint of the available space to reinforce their structure.

Based on the obtained results and the additional measures implemented, the conclusion is that the developed housing presents good mechanical integrity and has a high probability of passing the experimental free-fall tests.

5 EMC SIMULATIONS

5.1 Introduction

Miniaturized and high-frequency electronics are becoming highly integrated and have taken advantage of the exponential growth in the use of wireless communication over the past decades. Together however, the increase of noise and electromagnetic interferences (EMI) can compromise these sensible electronics. Making sure that the products will correctly operate, without disturbance, is a major concern for product developers. Consequently, more complexity on the development of enclosures is required, a conjugation on the use of better materials, from the electromagnetic performance, that affects the geometry of the product to comply with the requirements.

Sources of interference related to the vehicles are inverters and DC motors, as well the user's electronics operated by RF inside the car (mobiles, tablets, laptops) and other surrounding outside the car (communication towers, transmission lines, transformers, etc.). These sources can affect and interfere with sensible components necessary for the correct operation of modern cars, including multimedia devices. A common solution to protect these sensible components is to use a shield surrounding them.

EMI shields are conventionally metallic. However, the use of metal is disadvantageous to some fields, especially automotive, due to its higher cost and weight compared to other materials, besides the chance of corrosion – compromising the effectiveness. These have led to

the research of new materials applied to the EMI shielding, including conductive polymeric-based materials and polymeric composites.

Compared to metals, polymers present unique advantages such as lightweight, corrosion resistance, good processing performance and cost-competitiveness, and its electrical, magnetic, and mechanical properties can be adjusted in a wide range, which are substantial candidates for EMI shielding [9, 10].

Shielding materials must reflect or absorb incoming electromagnetic waves. Electrically conductive materials are both strong reflectors and strong absorbers, this is why metals are good shields. It is explained by the formulas and plane wave theory. Figure 15 illustrates the concept for shielding EM waves.

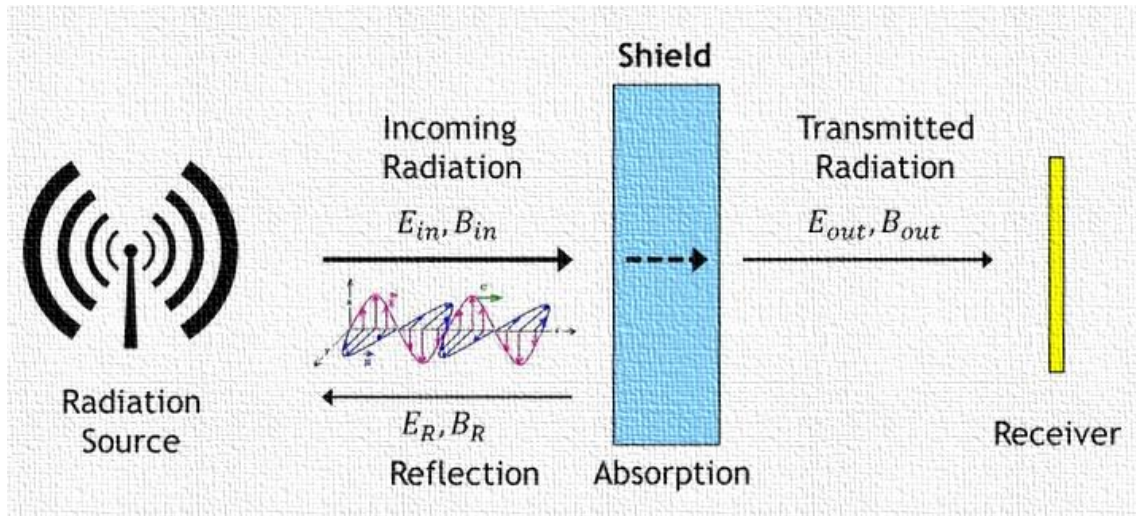


Figure 15 - Illustration of a shielding effect.

The shielding effectiveness (SE) is measured in decibels (dB) and represent the amount of power that passed through the shield, according to the Equation 1:

$$SE = 10 \log \left| \frac{P_{in}}{P_{out}} \right| \quad (1)$$

Traditionally, Schelkunoff's theory and its simplified Equation 2 is universally accepted to calculate the EMI of a shielding agent [11]. The total SE is the sum of reflection loss (SE_R), absorption loss (SE_A) and multiple reflection loss (SE_M) attenuation.

$$SE = SE_R + SE_A + SE_M \quad (2)$$

The plane wave theory is mostly used to calculate the SE related to the properties of the material used. The individual calculations of the parameters allow the understanding of a particular material with a specific thickness. In the reflection loss term, for example, the thickness of the material is irrelevant, as this loss is associated to the inherent impedance mismatch between free space and shielding material, which is a result of the interaction between charged particles

inside conductive material and electromagnetic field. Due to this impedance mismatch, the waves are reflected when they touch the surface of shield. For the absorption loss, however, the thickness and the conductivity of the material are both important, as it is the representative of the attenuation that occurs when a wave travels through the material once. Multiple reflection loss represents the internal reflections correction term. When the material is thick and conductive enough, it means, is much higher than the skin depth, this term can be simply neglected or when the SE_A term is found to be less than 10 or 6 dB [12].

The reflection loss SE_R is described in Equation 3 and the absorption loss SE_A in Equation 4. The multiple reflection loss SE_M is presented in Equation 5.

$$SE_R = 20 \log \left(\frac{Z_i}{4Z_s} \right) = 39.5 + 10 \log \left(\frac{\sigma}{2\pi f \mu} \right) \quad (3)$$

Where Z_i and Z_s are the impedances of the incident EM wave and material, respectively; σ and μ are the electrical conductivity and permeability, and f is the frequency of the EM wave. The thickness of the shield is t and δ is the skin depth.

$$SE_A = 8.68 \frac{t}{\delta} = 8.68 t \sqrt{\pi f \mu \sigma} \quad (4)$$

$$SE_M = 20 \log \left(1 - e^{-\frac{2t}{\delta}} \right) \quad (5)$$

Figure 16 presents comparisons of SE for materials with different conductivities at same thickness and Figure 17 shows the SE for different thickness of the same material.

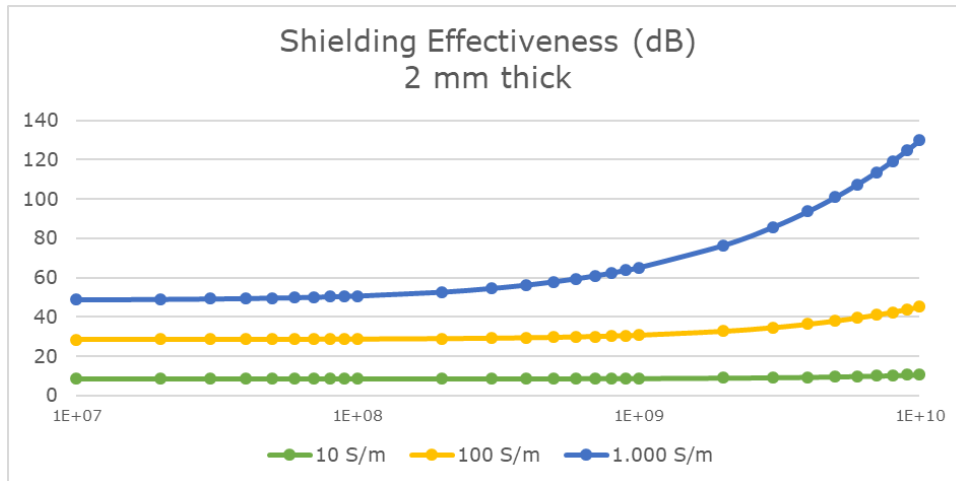


Figure 16 - Shielding effectiveness comparison for different conductivities.

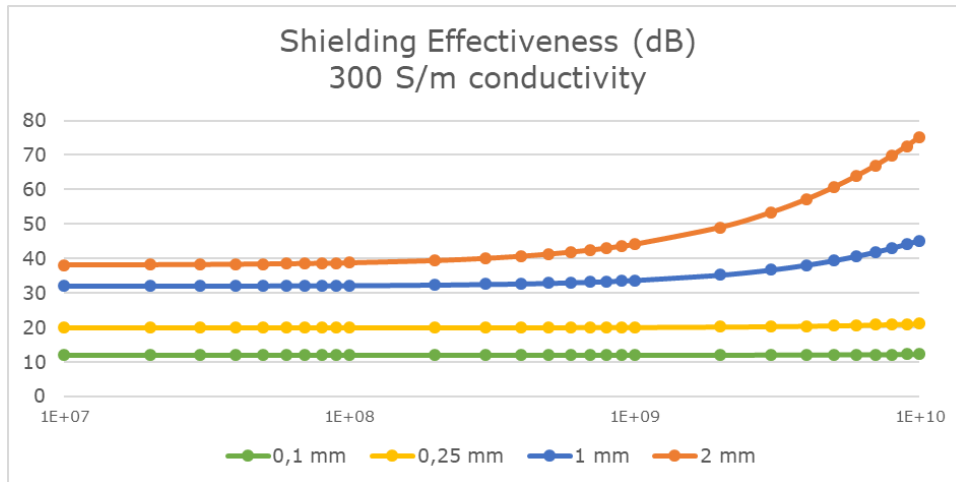


Figure 17 - Shielding effectiveness comparison for different thickness.

As seen, high values of conductivity result in better SE performance, and allow the thickness to be reduced. However, low values of conductivity tend to result in lower SE, so the thickness must be increased to compensate. This increase in thickness means more material, which means an increase in weight. These factors must be taken into consideration during the materials selection.

A SE below 20 dB is considered an ineffective EMI shielding. When the EMI SE is 30 dB, the material can block 99.9% of the incident radiation, which is considered a good shielding for several years. Today, the worldwide demand is a flexible, light, thinner and economic EMI shielding material required for electronic devices is over 20 dB – ideally over 40 dB [13, 14]. This value can be obtained with regular plastic with low content of additives [15].

The requirements for electronics usually are related to the operational frequency: the higher the frequency, the higher the effectiveness should be. Reference values are provided in Table 10.

Enclosure	Shielding Requirements
Notebook Computer	15-20 dB
Desktop Computer	15-20 dB
Cell Phone	70-90 dB
Cable tap	70-90 dB
Workstation/Server	30-40 dB

Table 10 - Approximate enclosure required shielding [16].

Various techniques can be used to perform the shielding, each with some variable performance and related to a cost. Figure 18 presents a scheme relating the relative cost vs. the shielding effectiveness of different methods.

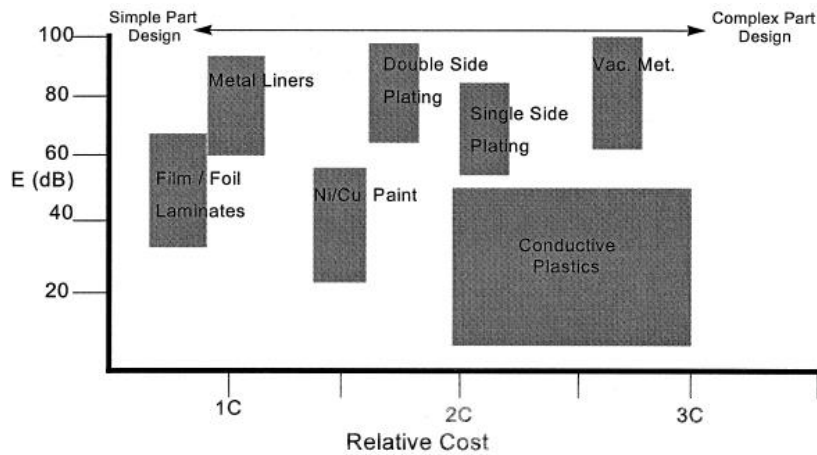


Figure 18 - Shielding effectiveness vs. relative costs of shielding methods [16].

5.2 Simulation Conditions

To predict the propagation and intensity of electromagnetic fields inside the enclosure, by calculating the electric field intensity and the shielding effectiveness, some numerical simulations are performed, and the maximum electric field values are analyzed to understand which enclosure internal points are more suitable to EM fields, which may lead to components damage or to erroneous functioning. For these simulations, commercial software Altair FEKO 2021 is used to build the models and simulate them.

To run the simulations, it is necessary to create the materials and assign them the correspondent electromagnetic properties. The CAD model used in the EM simulations comprehends the enclosure, the fan and ventilation grids, a rear panel and 3 internal PCBs. The PCBs are modeled as FR4, the fan grid and the rear panel are modeled as stainless steel, and the entire enclosure is modeled by two materials, namely, an electrically conductive polymer and the prepreg CFRTP.

In order to ease the results analysis and the location of the most critical points, the enclosure inner volume was divided into 9 individual volumes or zones, in 3 different layers. These layers are separated by the PCBs being two of them composed by 4 zones and the other one being a unique zone, as shown in Figure 19.

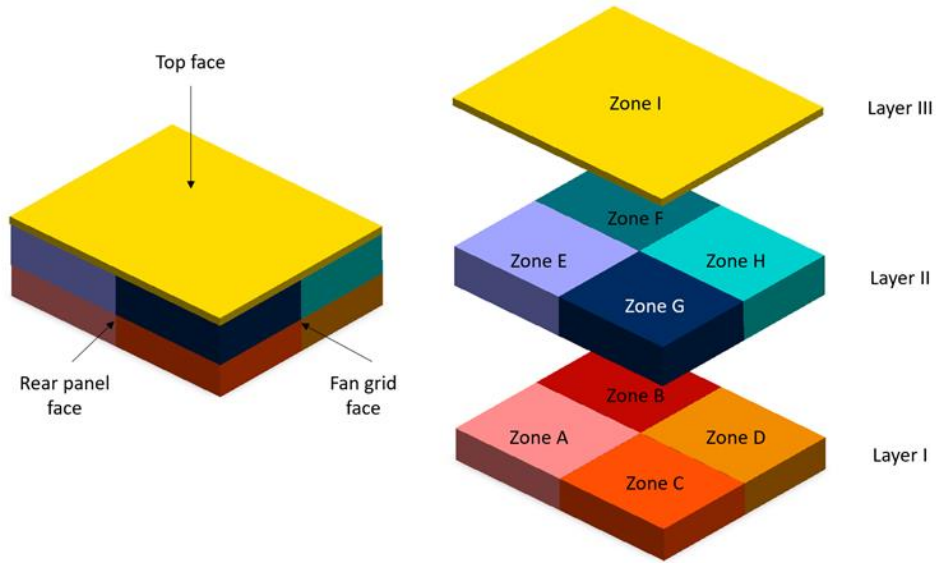


Figure 19 – Enclosure inner volume zones created for better understanding of the results.

In each simulation, it is requested to calculate the electric field (E-field) for 3348 points. 360 (8x9x5) points for each zone from A to H and 468 (13x18x2) points for zone I, spatially distributed as shown in Figure 20.

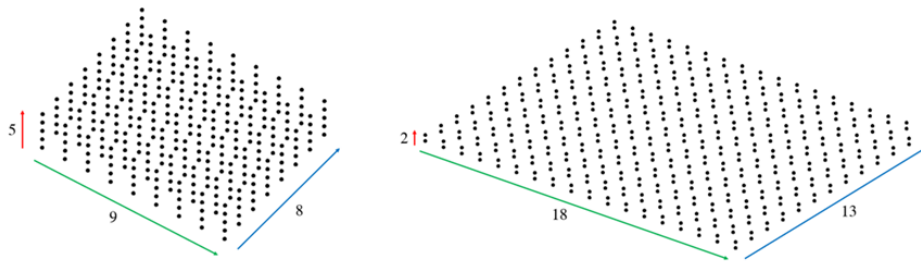


Figure 20 - Requested points for the E-field inside the enclosure.

Regarding the frequency domain, the simulations are evaluated for different frequencies, from 100 MHz to 3000 MHz, as this range comprises all the operating frequencies of the components inside the enclosure (GPS, Bluetooth, Wi-Fi bands, etc.). This range of frequencies is linearly separated into 30 frequencies, meaning a step of 100 MHz.

The mesh created to perform the simulations was defined by triangles flat elements with a global element size given by Equation 6 [17] where $\lambda_{(0min)}$ corresponds to the higher frequency which the enclosure is subjected to (3GHz). Therefore, the global element size, in millimeters, is:

$$\lambda_{(0min)}/12 = 100/12 \approx 8.328 \quad (6)$$

As a consequence, the meshes created for the simulations were composed of 52661 elements (Figure 21).

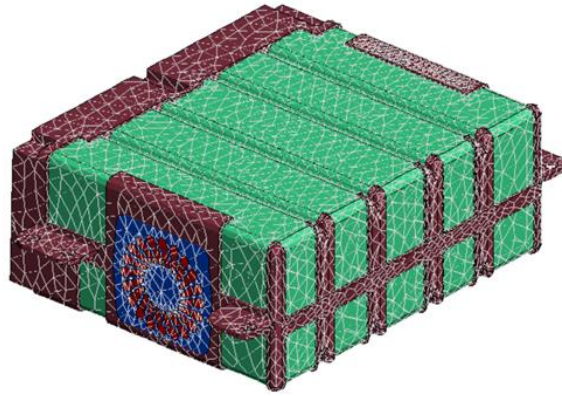
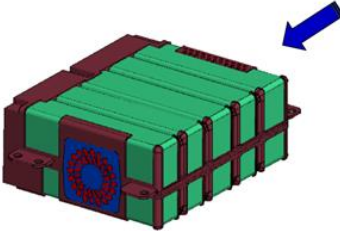
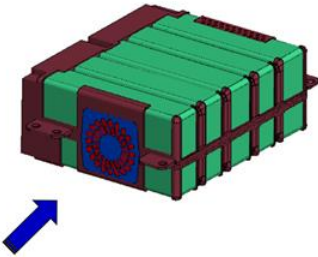
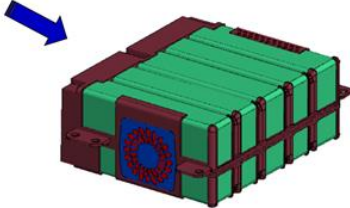
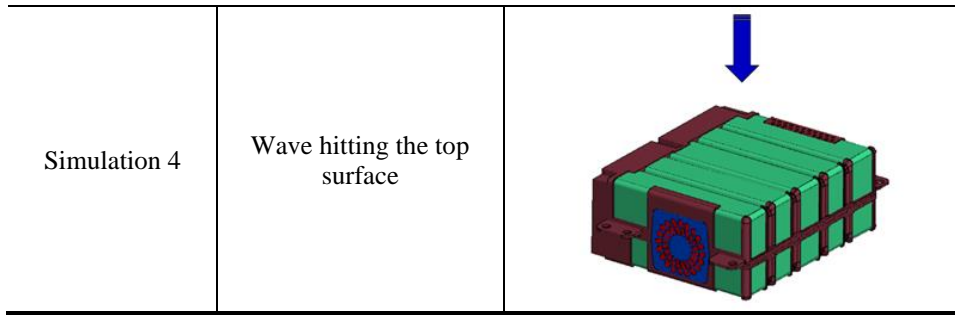


Figure 21 - Mesh created for the EMC simulations.

For each simulation, it is defined a planar wave hitting the enclosure with magnitude of 200 V/m, phase of 0° and the polarization orientation linear with an 0° angle. Four wave directions are evaluated to find the worst-case (Table 11). The Method of Moments (MoM) is used as solver.

Table 11 - Wave direction and incident surface in the enclosure.

Simulation #	Wave direction and incidence surface	Scheme
Simulation 1	Wave hitting the ventilation surface (air inlet)	
Simulation 2	Wave hitting the fan surface (air outlet)	
Simulation 3	Wave hitting the rear surface (rear panel)	



5.3 Results and Analysis

From the simulations, the maximum electric field values found for each zone are obtained, as presented in Figure 22.



Figure 22 - Max E-field found in all zones and frequencies, for each simulation.

In order to easily compare the obtained values, all the results are compiled in Figure 23. In Figure 23(a), it is exposed the maximum electric field values in each zone and in Figure 23b it can be seen the maximum E-field values by frequency, regardless of the zones.

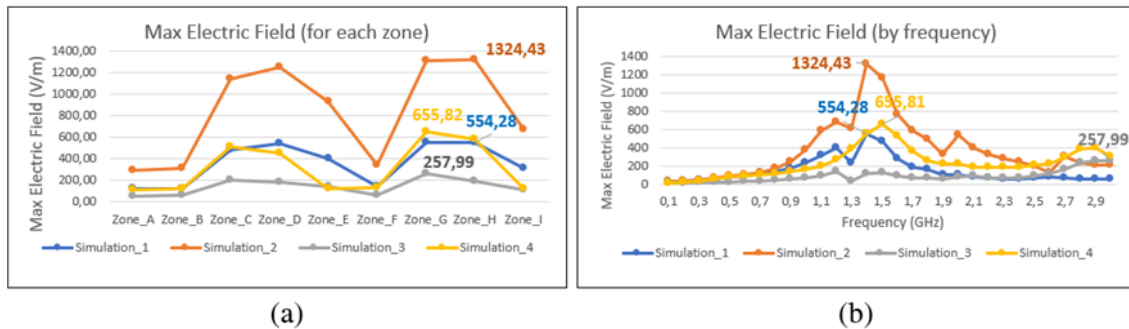


Figure 23 - Summary of the maximum values of E-field found in all simulations; (a) For each zone; (b) By frequency

The lowest values found are in simulation 3, where the incident wave hits the enclosure by the rear surface (rear panel). This is related to the fact that the rear face is made of stainless steel, a good conductive material, which can naturally work as a good shield due to the increased reflections, common in good conductive materials.

The highest value found in all the simulation occurred when the incident wave hits the enclosure through the air outlet (simulation 2). This, at a frequency of 1.4 GHz, the value corresponds to 1.3 kV/m, about 6 times higher than the magnitude of the incident wave (200 V/m). Further analysis shows that the partial zone where this value is found occurs near to the fan grid (Figure 24). The recommendations provided by the results are to maintain sensible components away from this particular zone or to change the openings design of the fan grid. These points are specially located near to enclosure openings to the exterior, in the zones C, D, E and F. Similarly, it is expected that the behavior and the electric field distribution was roughly the same if it was simulated with a wave source hitting the enclosure in the ventilation grid face. As such, the proximity of the ventilation grid shall also be avoided.

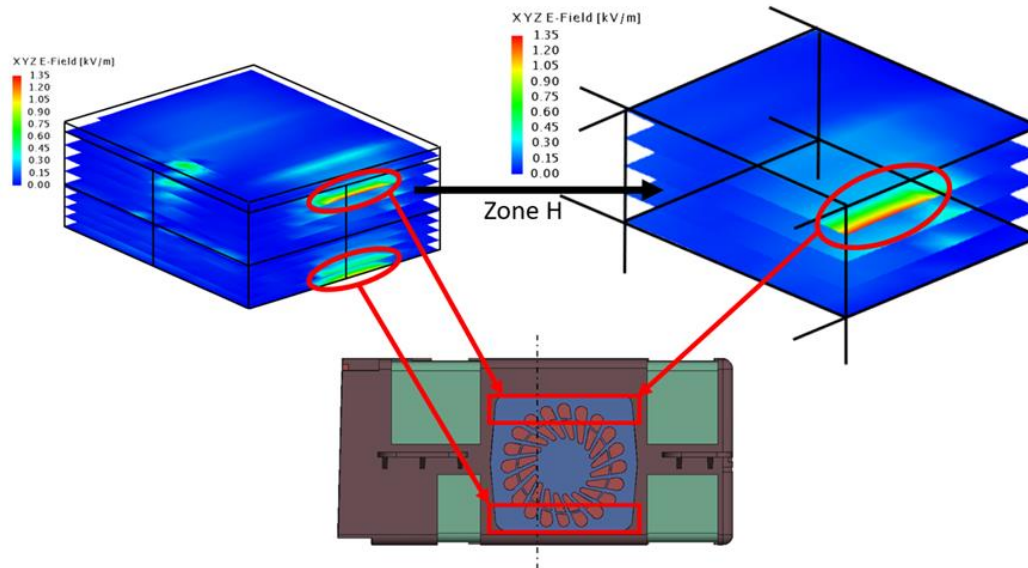


Figure 24 – Exemplar detailed position of the worst E-field points found in Simulation 2.

In almost every point of the inner enclosure volume, and for all frequencies, these maximum values are lower than the comparable values of the other simulations and they are generally much lower than the 200 V/m of the incident wave source.

6 EXPERIMENTAL ANALYSIS

The iterative simulation-guided design approach allowed the gain of insights into the product's strengths and weaknesses, thereby allowing the optimization of the electronic enclosure without constant physical testing. These numerical studies were a valuable tool for preliminary assessment and optimization during the design process. However, physical testing is typically required to ensure the real-world condition's performance, safety, and reliability.

Functional prototypes were produced, and performance tests were conducted focused on evaluating the thermal performance, mechanical robustness, and electromagnetic compatibility of the enclosure.

The experimental tests done were different from what was analyzed through the numerical simulation and served the sole purpose of validating the concept for conditions that will be applied during its use. Thus, it is not possible to directly compare the results obtained in the numerical simulations with the experimental tests since the applied conditions are different.

A comparison between experimental results and the predefined product specifications is made to demonstrate the reliability and suitability of the lightweight enclosure for the specific application.

6.1 Thermal

Through the numerical simulations previously described it was possible to evaluate the worst-case scenario, where all the components/heat sources attached to the PCBs were considered to be working. The concept was thus consecutively optimized until the observed temperatures of the components were below, or near, the limit stipulated in the datasheets.

The experimental tests consisted of the application of thermal load cycles, in a temperature cycle endurance test, while some of the components are monitored. At the end of this test, it is observed if these components are still functional and are not influenced by the temperature change. The components that are monitored are the critical ones, which represent a good global evaluation of the temperatures inside the enclosure.

For this test, 2 temperature cycles were considered, each cycle going firstly to a temperature of $-40\text{ }^{\circ}\text{C}$ (T_{\min}) and then to a temperature of $80\text{ }^{\circ}\text{C}$ (T_{\max}), following the profile presented in Figure 25, and having a temperature gradient of $4\text{ }^{\circ}\text{C}/\text{min}$. For temperature cycle tests, the concept, after having attained complete thermal equilibrium, shall be kept at the specified temperature values for a defined time, so that stress in the component can turn into strain. A component is considered to achieve complete thermal equilibrium at the point in time at which the temperature will not change by more than $3\text{ }^{\circ}\text{C}$ at any point of the component over the further course of time. In this case, the time considered for the tests was $15 + 225$ minutes.

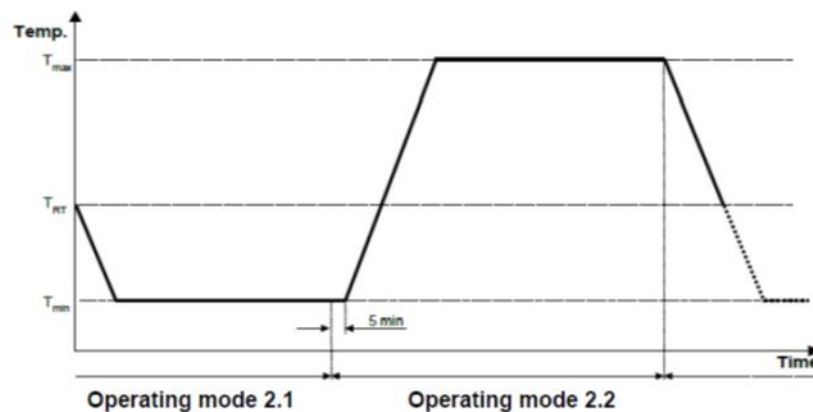


Figure 25 - Test temperature profile.

For this test, it is required that the concept is completely functional before and after the test and the provided thermocouple data shall demonstrate that the component dwells for 15 minutes, once it reaches $T_{\min} + 3\text{ }^{\circ}\text{C}$ and $T_{\max} - 3\text{ }^{\circ}\text{C}$. Figure 26 shows the temperatures monitored during the test, in the 9 thermocouples placed inside the concept.

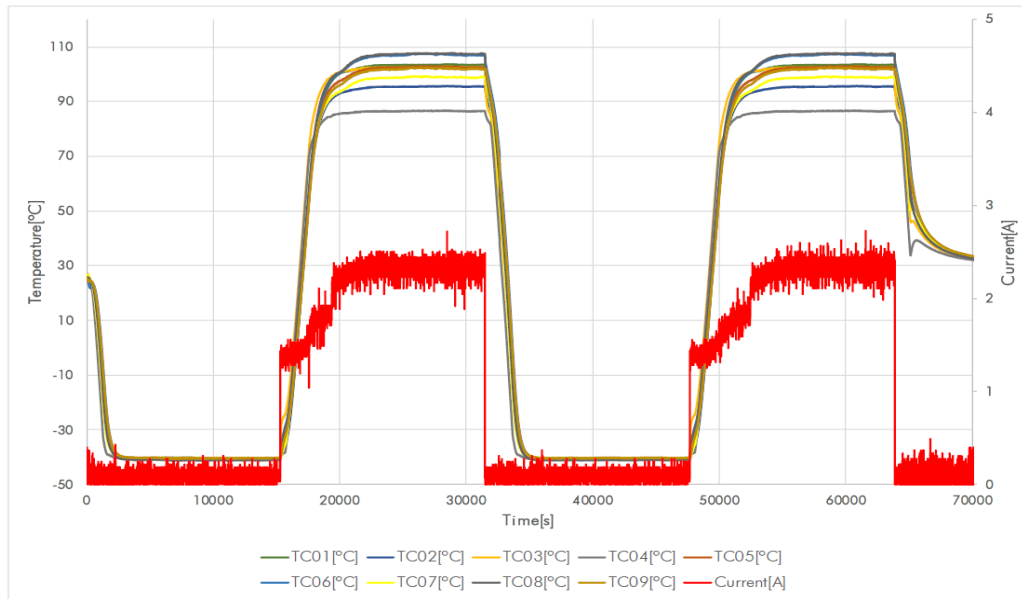


Figure 26 - Temperatures monitored during the test for the 9 thermocouples.

After the temperature cycle endurance test, a P03 test was done to evaluate if the prototype operates properly. This test consists of evaluating the power/consumption of the components throughout the temperature cycle tests, to check if there is any power/consumption fluctuation, which would mean that the components were being affected by the temperature changes. The results obtained in this test are presented in Table 12.

Table 12 – Results of the power/consumption fluctuation tests.

Sample	Current (RT°C) [A]			Current (65°C) [A]			Current (-40°C) [A]			Result [Class A]
	V _s :9V	V _s :12V	V _s :16V	V _s :9V	V _s :12V	V _s :16V	V _s :9V	V _s :12V	V _s :16V	
211040/0002	1,865	1,146	1,083	1,900	1,595	1,185	1,180	1,280	1,015	Ok

From the results obtained in this test, it was concluded that the concept can operate within the temperature range analyzed (-40 °C to 80 °C) without significant changes in the behavior of the components. Furthermore, a visual inspection was also performed, and no visual changes were found.

6.2 Vibration

The vibration test verifies the component's functionality after subjecting it to the vibration profile based on component location. The vibration profiles are accelerated test stresses to simulate vibrations experienced by components due to road conditions while driving and/or engine cranking. To successfully pass the tests, the equipment should show no visual damage after the tests.

In the test made to the prototype, the purpose was to determine the unit resistance to random vibration under climatic conditions. The climatic conditions of the test are presented in Figure 27. Each thermal cycle has a duration of 8 hours and a minimum operation temperature of -40°C and

a maximum operation temperature of 65°C. The vibration shaker was programmed for the random vibration profile shown in Figure 28, which represents a simplified version of the profile used in the numerical simulation and has a frequency range from 5 Hz to 2000 Hz. Three tests were carried out, one for each vibration axis (X, Y, and Z), resulting in 24h duration for each sample tested.

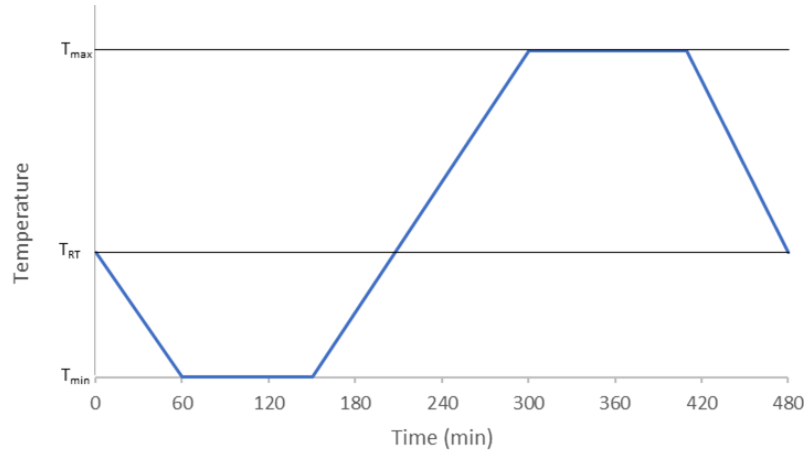
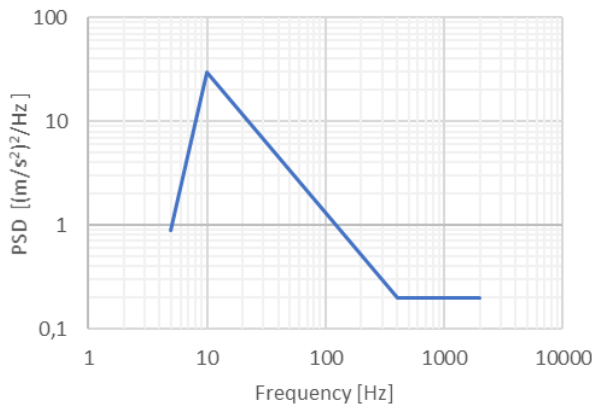


Figure 27 - Climatic profile: where, T_{min}= -40°C and T_{max} = + 65°C.



Frequency [Hz]	PSD [(m/s ²) ² /Hz]
5	0.884
10	30
400	0.2
2000	0.2

Figure 28 - Vibration profile applied in vibration test.

After the test, a visual inspection was conducted and no sign of breakage, cracks or other malfunctions were shown in the samples. Figure 29 shows the functional checking of the samples after the test.

Sample	Current (RT°C) [A]			Current (65°C) [A]			Current (-40°C) [A]			Result [Class A]
	V _s =9V	V _s =12V	V _s =16V	V _s =9V	V _s =12V	V _s =16V	V _s =9V	V _s =12V	V _s =16V	
01	1.716	1.272	1.466	1.178	1.869	1.097	1.751	1.289	1.204	Ok
03	0.993	0.970	0.994	1.025	1.089	1.061	0.884	1.678	1.543	Ok
05	0.071	0.067	0.071	0.066	0.059	0.057	0.071	0.067	0.070	Ok
06	0.067	0.059	0.057	0.068	0.060	0.058	0.066	0.059	0.057	Ok

Figure 29 - Functional test results for vibration.

6.3 Free-fall

This test simulates the free fall of a device to the floor, as it may occur during the complete process chain until the intended mounting on the vehicle. The part under test falls from 1m height to the concrete ground floor on the 3 directions (x, y, and z) on both sides.

The units after the test are inspected to verify the existence of any damage or pre-damage and shaken to check if it has rattling noise prevention from any electronic component element displacement or crack.

Figure 30 shows the physical damages in the enclosure and a comparison with the critical zones identified in the numerical study presented previously.

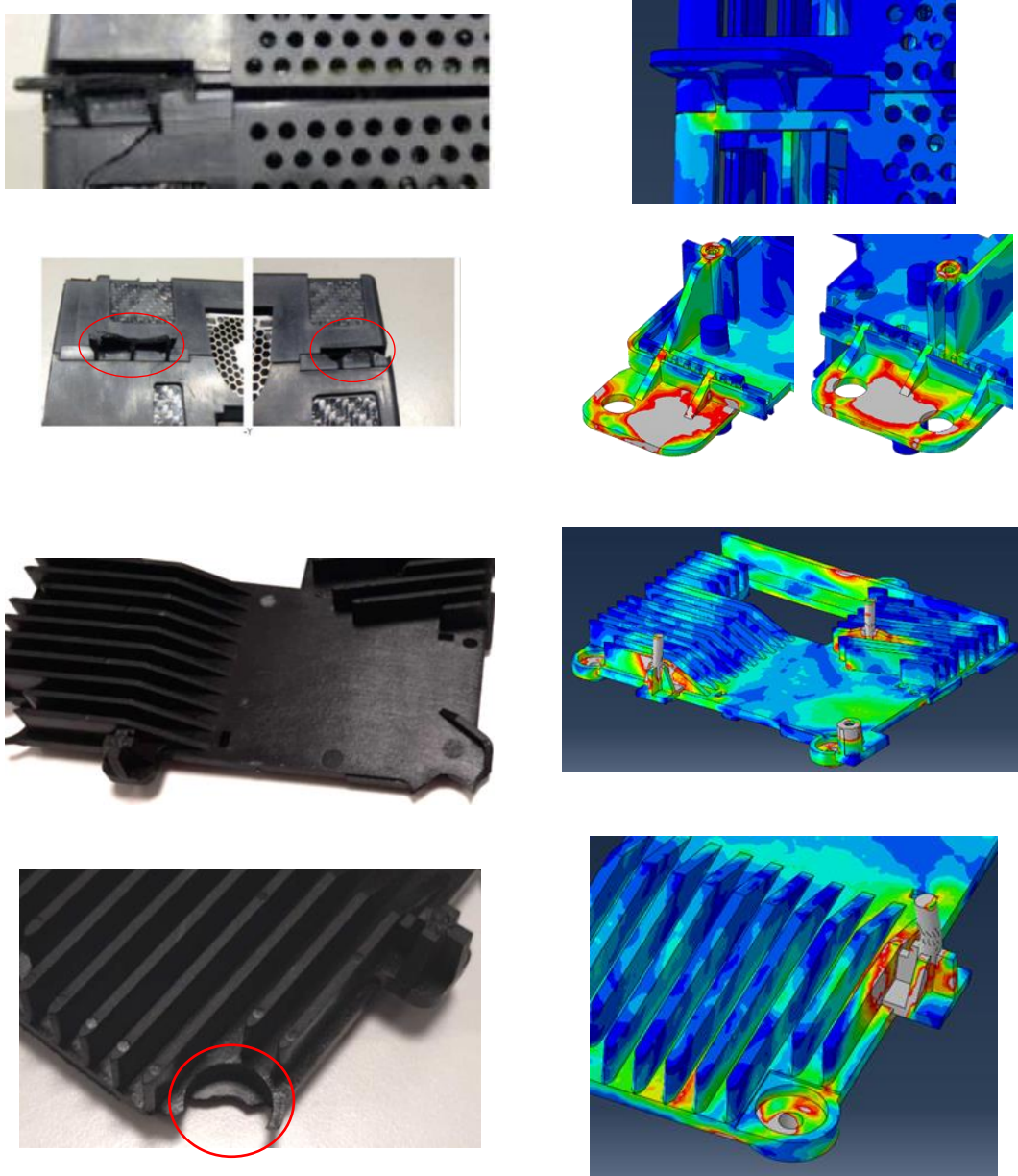


Figure 30 - Failure detected in the components of the enclosure after the free fall test and comparison with the numerical simulation.

The tested samples present some physical damage and breaks in features like the brackets designated to do the fixation in the car, some fissures at the corners close to the brackets and a slight opening on the backside.

A few rattling noises were heard, and after opening the enclosure, it was discovered that they were caused by broken positioning pins in the heatsink. These failures did not compromise the electronic behavior of the units, but the parts were reinforced to prevent this type of failures on the following steps of product development validation. The back opening is also related to the breakage of the bosses of the intermediate part that are connected to the top part.

It can be noticed the alignment between the impact-induced damage in the different components and the simulation predictions.

Despite the identified damages, no damage was observed in the electronic parts.

6.4 EMC

Numerical simulations allowed to understand the behavior of the E-fields inside the enclosure for different frequencies. The values found in those simulations drove us to a confidence level about the EMC requirements fulfillment, defined by the internal customer standards. Hence, the final polymeric device was experimentally tested according to the CISPR 25 (out EMC studio for development purposes). The results were evaluated for different frequencies, relating different bands of operation: from 30 - 1000 MHz (for FM, DAB and TV bands) and from 1 - 3 GHz (for GPS and Wi-Fi bands), and were compared with the results of the tests made to the original metallic device. Figure 31 and Figure 32 present the comparison for the E-field levels of the previous enclosure (metallic) and the final concept developed (polymeric).

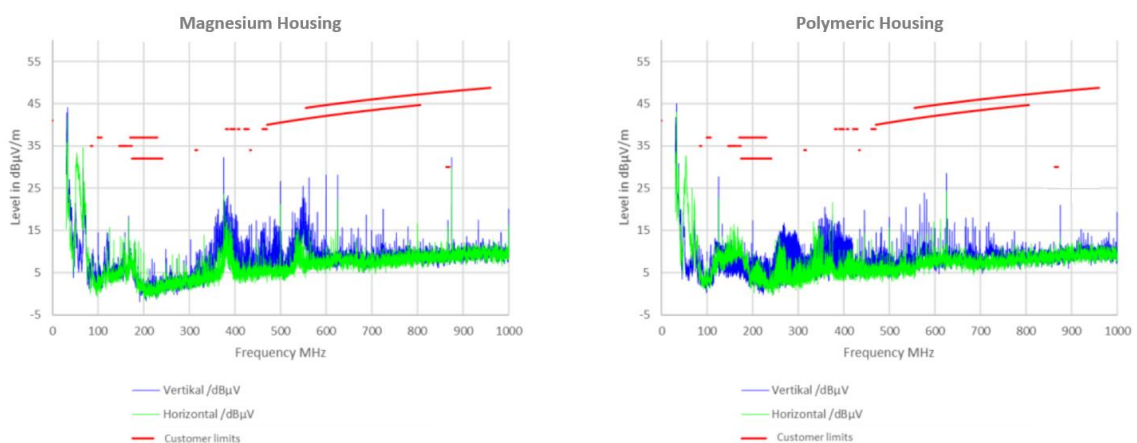


Figure 31 - E-field levels found for a) Magnesium and b) Polymeric housing at low frequencies 30 – 1000 MHz.

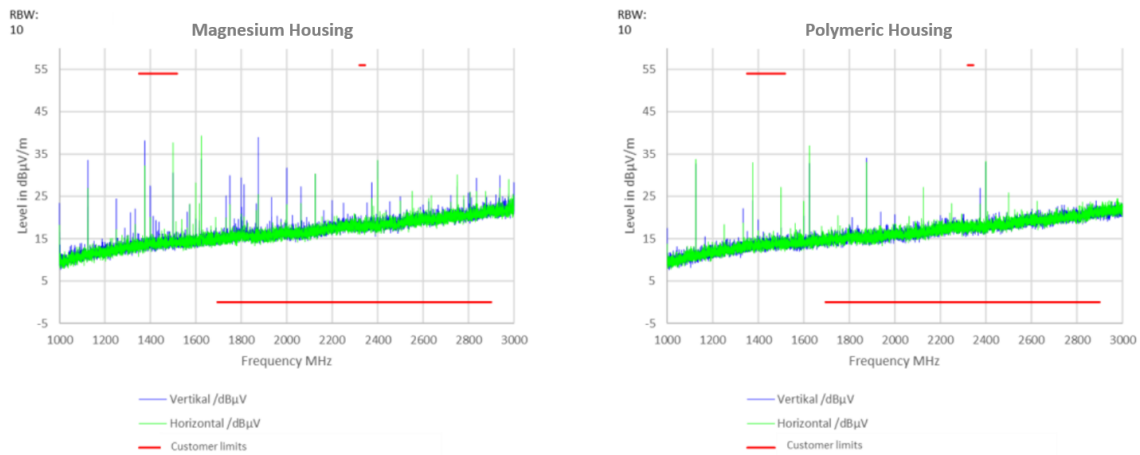


Figure 32 - E-field levels found for a) Magnesium and b) Polymeric housing at high frequencies 1 - 3 GHz.

The results show that the polymeric housing has a more homogeneous spectrum along all the frequencies. Some harmonic peaks at certain frequencies were minimized, comparatively to the magnesium housing. More important, all the values found experimentally are below the maximum levels (in red in Figure 31 and Figure 32) for the bands specified by the customer.

Additionally, to have a real overview of the attenuation capacity of the enclosure, the E-field levels were measured with the device without the top housing (Figure 33). The results evidence the effectiveness of the enclosure, since that, without the top cover, the values found are very close to the limit values for certain frequency bands.

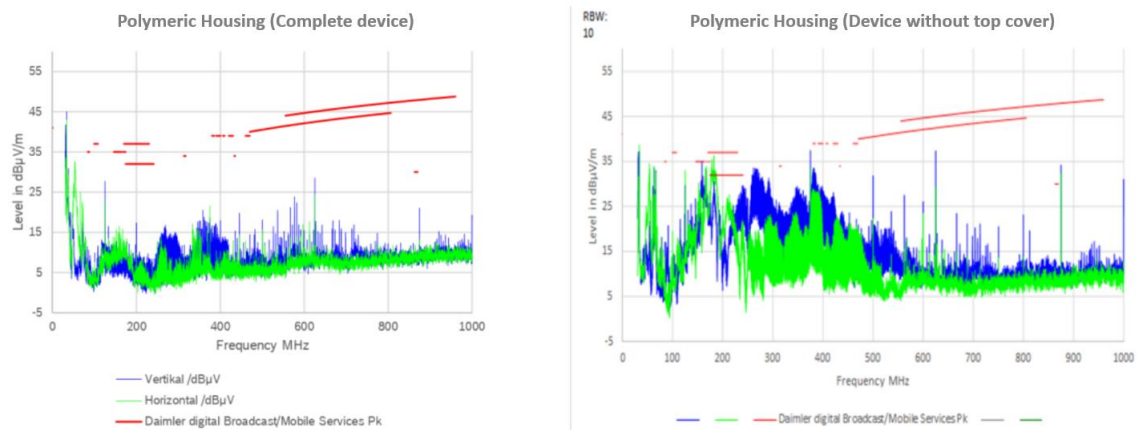


Figure 33 - EMC results for a) complete device b) Device without top housing at frequencies range from 0 to 1000 MHz.

Finally, the experimental analysis allows the assurance that the developed product is compatible electromagnetically and all the relevant requirements are fulfilled.

7 CONCLUSIONS

In this study and work, we developed a lightweight electronic enclosure with the aim of reducing weight by replacing conventional metallic components with functional thermoplastics and composites. Our product design and development approach places significant emphasis on simulations, playing a crucial role in material selection, geometry optimization, and ensuring adherence to requirements. Thermal, mechanical, and electromagnetic shielding simulations were conducted, generating results that were iteratively incorporated into new CAD releases, progressively optimizing the geometry until reaching a final design that met all requirements.

The chosen final concept demonstrated satisfactory results in fulfilling the specified requirements, particularly in thermal behavior. Thermal simulations indicated a significant decrease in temperatures across all major volumes and components, demonstrating an appropriate response to the heat generated by power sources/components. Notably, certain components exhibited elevated temperatures in simulations, which were deemed non-problematic since the scenario—simultaneous operation of all heat sources—assumed a condition unlikely to occur in reality. Numerical simulations also assessed the enclosure's structural integrity and performance under challenging conditions, including vibration attenuation, maintenance of structural integrity under defined conditions, and resistance to displacements and accelerations that could affect internal components. Free fall simulations identified weak points and stress-prone areas, demonstrating the enclosure's ability to absorb and dissipate impact energy, safeguarding internal electronic components. Electromagnetic compatibility (EMC) simulations revealed the enclosure's effectiveness in attenuating incident electromagnetic fields and identified critical points for assembly of internal electronic components.

Experimental tests, while not directly comparable to numerical solutions due to differing conditions, validated the enclosure's thermal performance, structural integrity, and electromagnetic compatibility in realistic scenarios. Thermal experimental tests validated the enclosure's ability to withstand expected thermal loads during its life cycle. Structural tests demonstrated satisfactory performance under random vibrations and drop conditions, preserving the integrity of internal components. EMC tests, performed in a range of frequencies between 30MHz to 3GHz, confirmed the polymeric concept's compliance with project requirements, exhibiting levels below specified limits and outperforming the metallic baseline in certain frequencies. The results collectively endorse the effectiveness of our simulation-driven approach in optimizing the electronic enclosure for enhanced performance, reduced weight, and improved environmental compatibility.

Moreover, the initial specification of weight reduction was checked based on prototypes production and measurement. The metallic baseline weighed 911g and the final composite concept presents a weight of 606g, which means a 33% weight reduction. |

[FC2][FC3]3434Overall, the successful outcomes of the developed electronic enclosure validate the effectiveness of the simulation-driven approach employed for product optimization. Through the seamless integration of simulations, the study demonstrates the efficient evaluation of multiple design iterations, resulting in a notable reduction in both development time and costs. The obtained results conclusively indicate that the final design not only meets the specified requirements for performance and weight but also holds promising potential for cost and environmental impact reduction. Additionally, the validated design ensures sufficient protection for enclosed electronic components. These results demonstrate the robustness of simulation-driven methodologies in achieving optimized product outcomes across several critical parameters, thereby contributing to enhanced efficiency and resource conservation in the development process.

8 REFERENCES:

[1] Gupta, M. K., Singhal, V. (2022). **Review on materials for making lightweight vehicles.** Materials today proceedings, Vol 56, Part 2, pp 868-872.

[2] Lyu, M-Y., Choi, T. G. (2015). **Research trends in polymer materials for use in lightweight vehicles.** Int. J of Precision Eng and Manufacturing, 16, pp 213-220.

[3] Mallick, P.K. (2021). **Materials, design and manufacturing for lightweight vehicles.** Chapter 5 – thermoplastics and thermoplastic-matrix composites for lightweight automotive structures. pp 187-228.

[4] Singha, Nayan & Deb, Mousumi & Mahapatra, Manas & Mitra, Madhushree & Chattopadhyay, Pijush. (2020). **Smart Lightweight Polymer Composites.** 10.1201/9780429244087-8.

[5] Yao, Yuanyuan & Jin, Shaohua & Zou, Haoming & Li, Lijie & Ma, Xianlong & Lv, Gang & Gao, Feng & Lv, Xijuan & Shu, Qinghai. (2021). **Polymer-based lightweight materials for electromagnetic interference shielding: a review.** Journal of Materials Science. 56. 10.1007/s10853-020-05635-x.

[6] Johnson, R. & Evans, John & Jacobsen, Peter & Thompson, J.R.R. & Christopher, Mark. (2004). **The Changing Automotive Environment: High-Temperature Electronics.** Electronics Packaging Manufacturing, IEEE Transactions on. 27. 164 - 176. 10.1109/TEPM.2004.843109.

[7] Viswanathan, S., Sridharan, K., and Gupta, N. (2023). **Influence of Uncertain Factors on Automotive Electronics Thermal Simulation.** SAE Technical Paper 2023-01-0766, <https://doi.org/10.4271/2023-01-0766>.

[8] Martins, L., Barbosa, C., Silva, S., Bernardo, P., Dias, G., Pontes, A. (2021). **Effect of processing conditions on electromagnetic shielding and electrical resistivity of injection moulded PBT compounds.** Polymer Engineering and Science 2021, 2576-2588, <https://doi.org/10.1002/pen.25784>

[9] Zhang, Y., Qiu, M., Yu, Y., Wen, B., Cheng, L. (2017). **A Novel Polyaniline-Coated Bagasse Fiber Composite with Core-Shell Heterostructure Provides Effective Electromagnetic Shielding Performance.** ACS Applied Materials & Interfaces 2017 9 (1), 809-818. doi: 10.1021/acsami.6b11989

- [10] Kar, G.P., Biswas, S., Rohini, R., Bose, S. (2015). **Tailoring the dispersion of multiwall carbon nanotubes in co-continuous PVDF/ABS blends to design materials with enhanced electromagnetic interference shielding**. *J. Mater. Chem. A* 2015 (15), 7974–7985. doi: 10.1039/C5TA01183C
- [11] Schelkunoff, S.A. (1943). **Electromagnetic waves**. Van Nostrand, Princeton, NJ.
- [12] Phipps, K. (2008). **TC-4 Studies Shielding Theory and Practice**. 2008 IEEE International Symposium on Electromagnetic Compatibility, Detroit, MI, USA.
- [13] Park, D.H., Lee, Y.K., Park, S.S. et al. (2013). **Effects of hybrid fillers on the electrical conductivity and EMI shielding efficiency of polypropylene/conductive filler composites**. *Macromol. Res.* 21, 905–910. doi:10.1007/s13233-013-1104-8
- [14] Tiwari, Alavya & Tiwari, Arushi & Bhatia, Arpit & Chadha, Utkarsh & Kandregula, Satvik & Selvaraj, Senthil Kumaran & Bhardwaj, Preetam. (2022). **Nanomaterials for Electromagnetic Interference Shielding Applications: A Review**. *Nano*. 17. 10.1142/S1793292022300018
- [15] Chen, S.-C., Chien, R.-D., Lee, P.-H. and Huang, J.-S. (2005). **Effects of molding conditions on the electromagnetic interference performance of conductive ABS parts**. *J. Appl. Polym. Sci.*, 98: 1072-1080. <https://doi.org/10.1002/app.22241>
- [16] Markham, D. (1999). **Shielding: quantifying the shielding requirements for portable electronic design and providing new solutions by using a combination of materials and design**. *Materials & Design* 21.1 pp. 45-50, ISSN 0261-3069. [https://doi.org/10.1016/S0261-3069\(99\)00049-7](https://doi.org/10.1016/S0261-3069(99)00049-7).
- [17] Altair Engineering, Inc. (2022) **Automatic meshing for faces and edges**. (Online). Available in: https://help.altair.com/feko/topics/feko/user_guide/appendix/mesh_automatic_faces_edges_feko_r.htm

9 APPENDIX A – POWER OF THE HEAT SOURCES CONSIDERED IN THE THERMAL SIMULATIONS

Heat source	Power (mW)	Location	Power (W)	Area (m ²)	Power density (W/m ²)
1, 2	Not considered	PCB B top	-	-	-
3	1580	PCB C top	1.58	3.31E-07	4.77E+06
4, 5	750		0.75	1.82E-07	4.11E+06
6	975		0.975	5.91E-08	1.65E+07
7	550	PCB C bottom	0.55	1.97E-07	2.79E+06
8	3400		3.4	4.97E-07	6.84E+06
9, 10, 11, 12	1600	PCB A top	1.6	1.33E-07	1.20E+07
13	2000		2	6.76E-07	2.96E+06
14	600	PCB A bottom	0.6	7.47E-08	8.04E+06
15	7000		7	2.03E-07	3.46E+07
16	1175	PCB C top	1.175	5.20E-08	2.26E+07
17	687		0.687	5.79E-08	1.19E+07
18	550		0.55	5.79E-08	9.50E+06
19	820	PCB B top	0.82	5.09E-07	1.61E+06
20, 21	2000		2	1.05E-06	1.91E+06
22	6400		6.4	4.88E-07	1.31E+07
23	1700		1.7	4.88E-07	3.48E+06
24	400		0.4	1.66E-08	2.42E+07
25	3400		3.4	1.66E-08	2.05E+08
26	1480		1.48	2.58E-08	5.75E+07
27	1370		1.37	3.34E-08	4.10E+07
28	1570		1.57	2.66E-08	5.90E+07
29	1500		PCB A top	1.5	3.34E-08
30	390	PCB C top	0.39	5.92E-08	6.59E+06
32	3190	PCB B top	3.19	4.83E-07	6.60E+06
33	200	PCB C top	0.2	6.30E-08	3.17E+06
34	200	PCB C top	0.2	6.12E-08	3.27E+06
35	1290	PCB B top	1.29	1.21E-07	1.07E+07
36	300	PCB A top	0.3	2.21E-08	1.36E+07
37	700		0.7	7.35E-08	9.52E+06
38, 40	300		0.3	1.04E-08	2.89E+07
39	500		0.5	1.84E-08	2.71E+07
41	300		0.3	2.21E-08	1.36E+07
42	330	PCB A bottom	0.33	1.35E-07	2.44E+06
43, 44	300		0.3	1.46E-07	2.05E+06
45	1600	PCB A top	1.6	2.45E-07	6.54E+06
46	200		0.2	1.88E-08	1.06E+07
47	1200		1.2	3.19E-08	3.77E+07
48	600	PCB B top	0.6	5.12E-08	1.17E+07
49, 50	1730	PCB C bottom	1.73	4.79E-08	3.61E+07
51	940	PCB C top	0.94	4.65E-07	2.02E+06
52, 54	1500		1.5	1.50E-07	1.00E+07
53	13750		13.75	5.42E-07	2.54E+07
55	940		0.94	4.65E-07	2.02E+06
56	2440	PCB B top	2.44	4.91E-07	4.97E+06
57	125	PCB C top	0.125	9.80E-09	1.28E+07
58	250		0.25	1.81E-08	1.39E+07
59	80	PCB B top	0.08	4.80E-08	1.67E+06
60	10		0.01	2.16E-08	4.62E+05
61	80		0.08	3.38E-08	2.37E+06
62	300	PCB A bottom	0.3	6.70E-08	4.48E+06

63	170	PCB C top	0.17	3.48E-08	4.88E+06
64	36	PCB C bottom	0.036	1.03E-07	3.48E+05
65	144		0.144	5.83E-08	2.47E+06